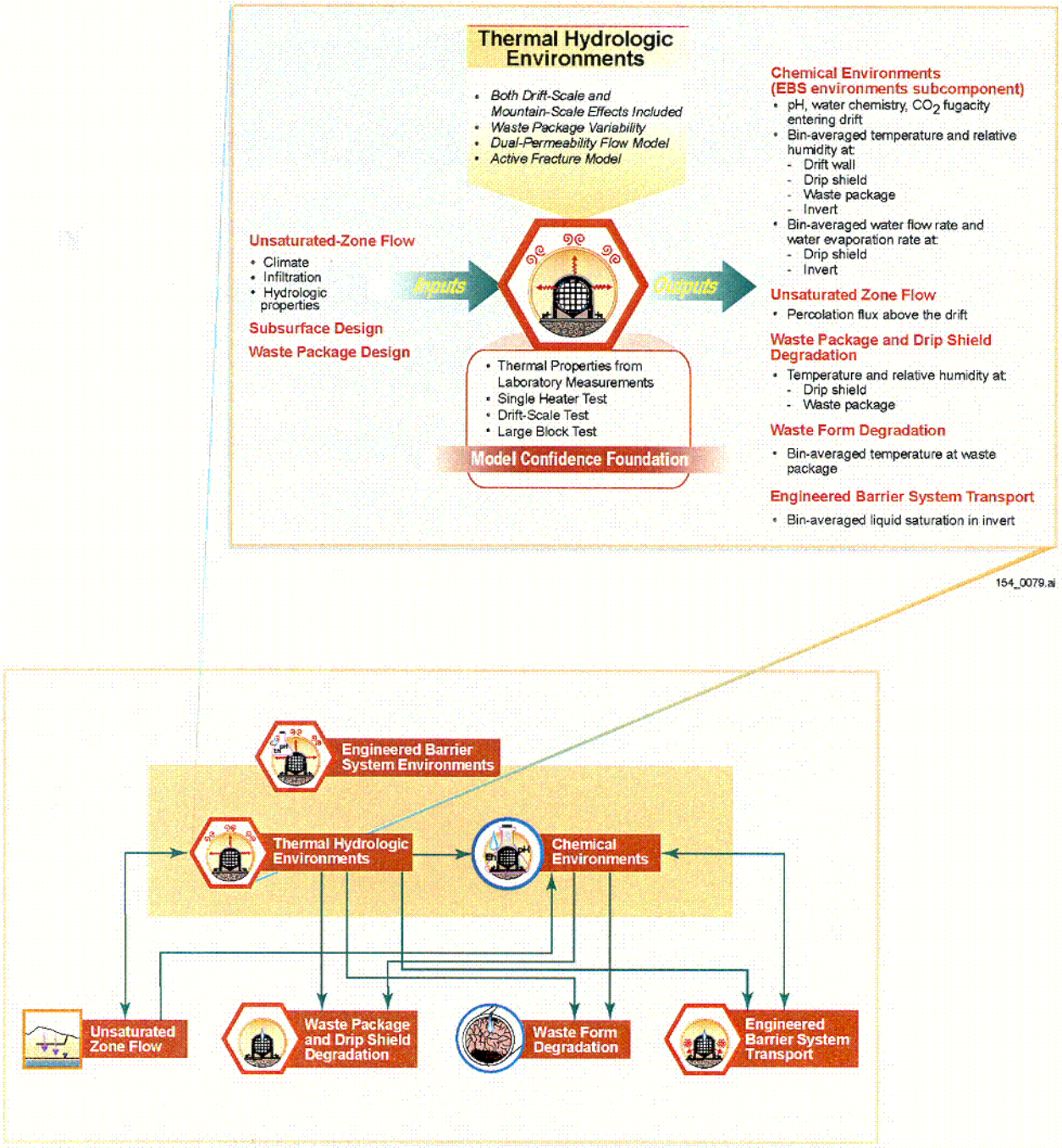

154_0079.ai

Source: CRWMS M&O 2000 [DIRS 153246], Figure 3.3-7.

Figure 5.2-1. Relationship of the Multiscale Thermal-Hydrologic Model to Other Models

C01

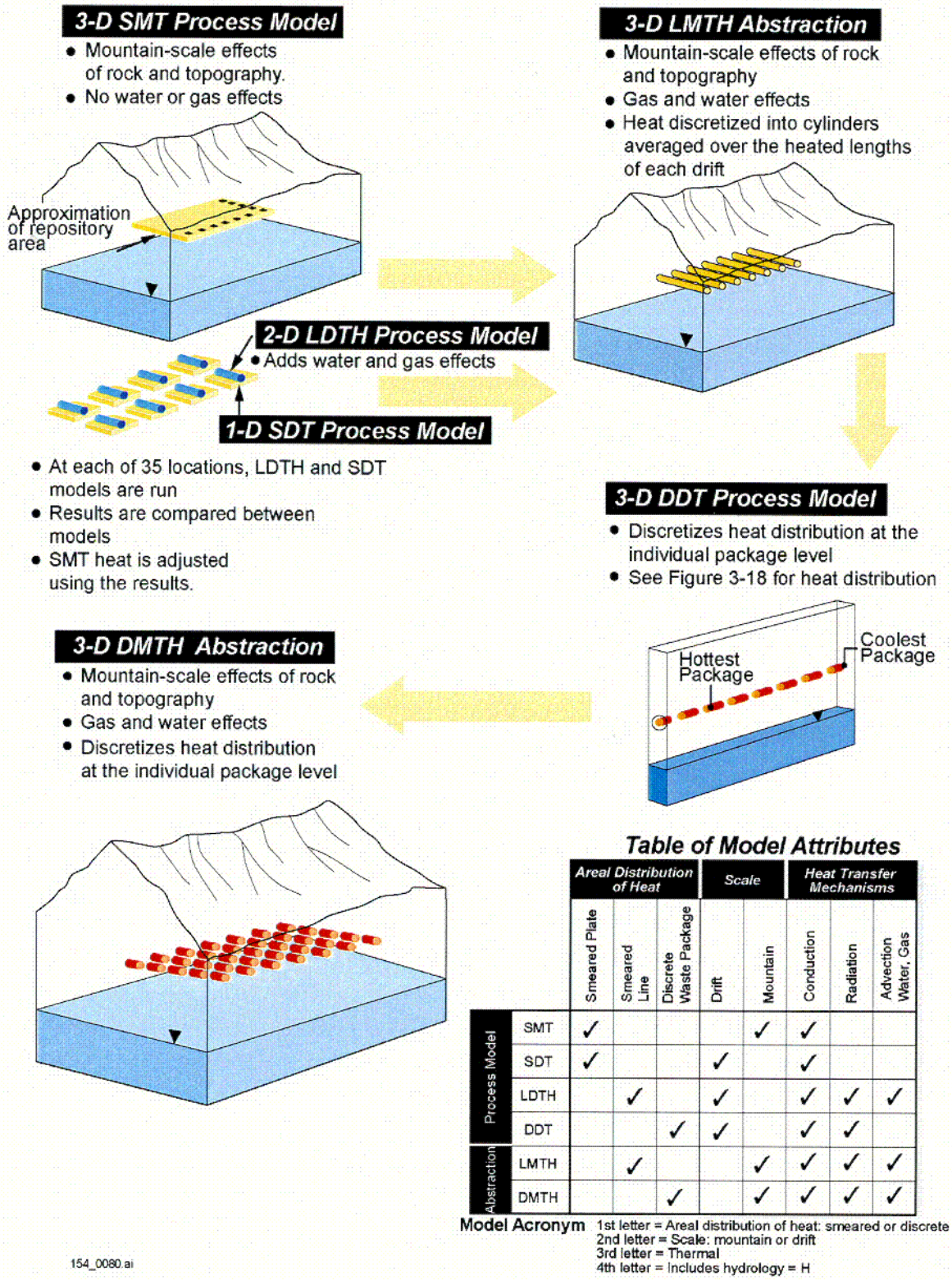

		Areal Distribution of Heat			Scale		Heat Transfer Mechanisms		
		Smeared Plate	Smeared Line	Discrete Waste Package	Drift	Mountain	Conduction	Radiation	Advection Water, Gas
Process Model	SMT	✓				✓	✓		
	SDT	✓			✓		✓		
	LDTH		✓		✓		✓	✓	✓
	DDT			✓	✓		✓	✓	
Abstraction	LMTH		✓			✓	✓	✓	✓
	DMTH			✓		✓	✓	✓	✓

154_0080.ai

Source: Adapted from CRWMS M&O 2000 [DIRS 149862], Figure 1-1.

Figure 5.2-2. Illustration of the Multiscale Thermal-Hydrologic Model

C02

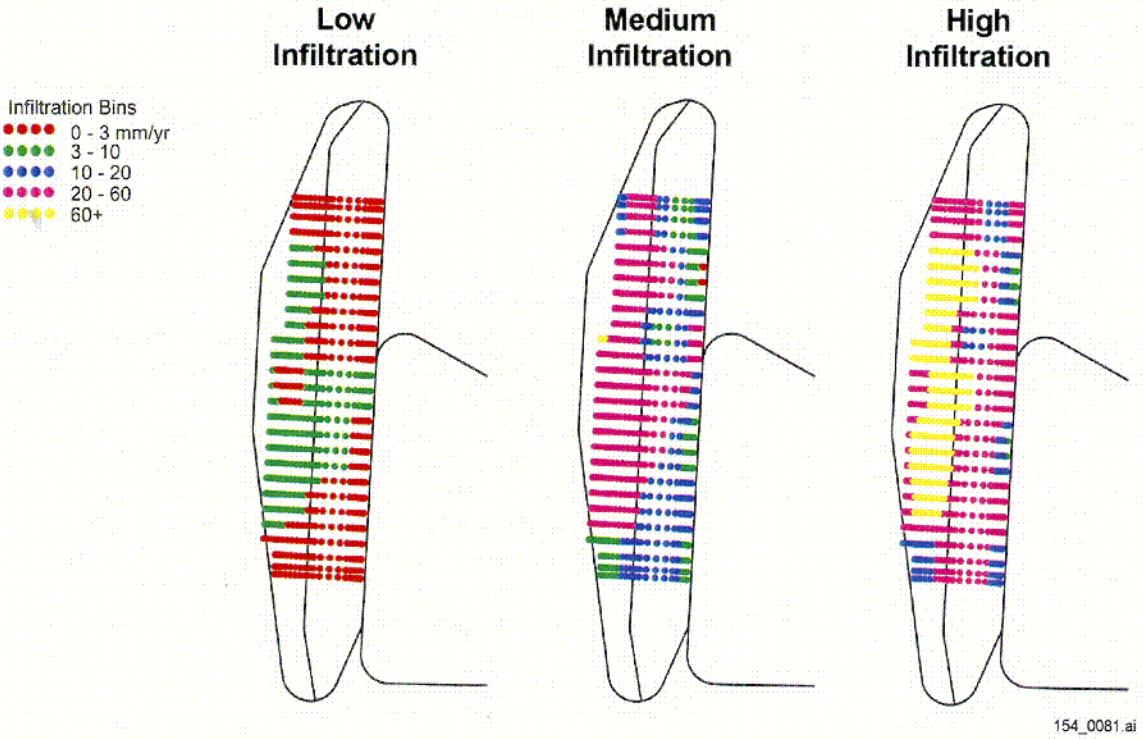

154_0081.ai

Source: CRWMS M&O 2000 [DIRS 153246], Figure 3.3-3.

Figure 5.2-3. Locations at Which Thermal-Hydrologic Parameters are Calculated by the Multiscale Thermal-Hydrologic Model

C03

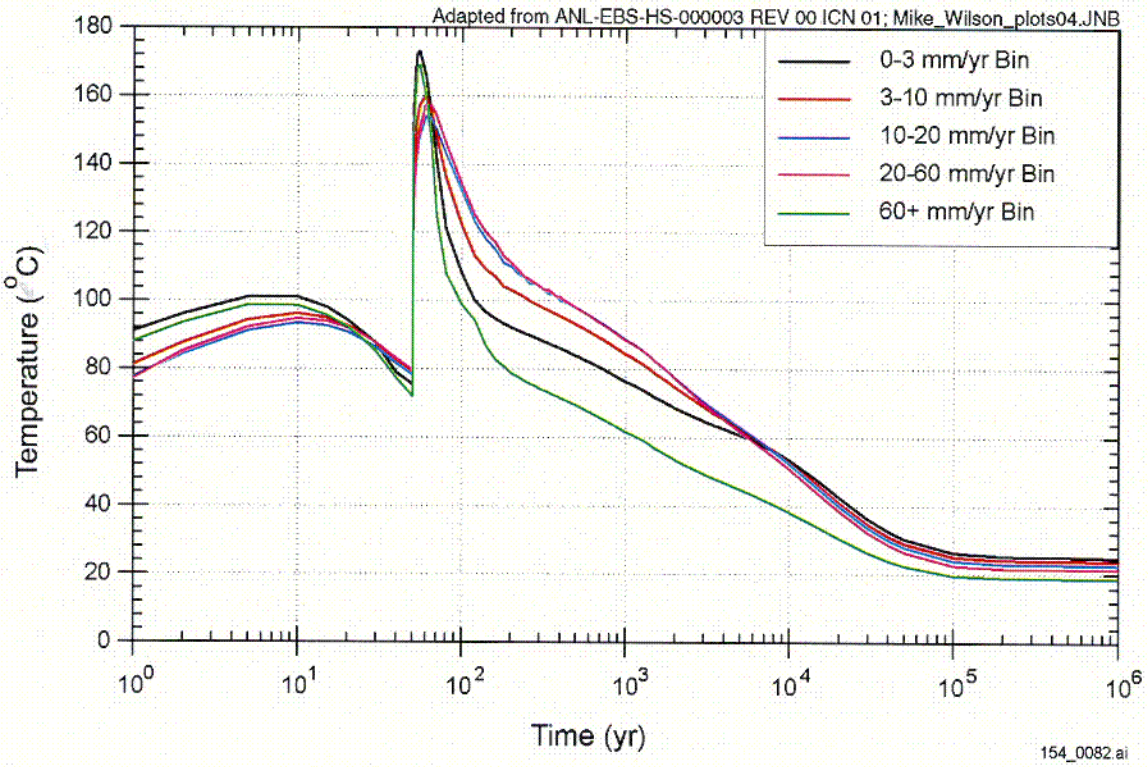

154_0082.ai

Source: CRWMS M&O 2000 [DIRS 153246], Figure 3.3-9.

NOTE: Commercial spent nuclear fuel temperature histories averaged into infiltration-level bins. Data for medium overall infiltration into the mountain.

Figure 5.2-4. Waste Package Temperature Histories

C04

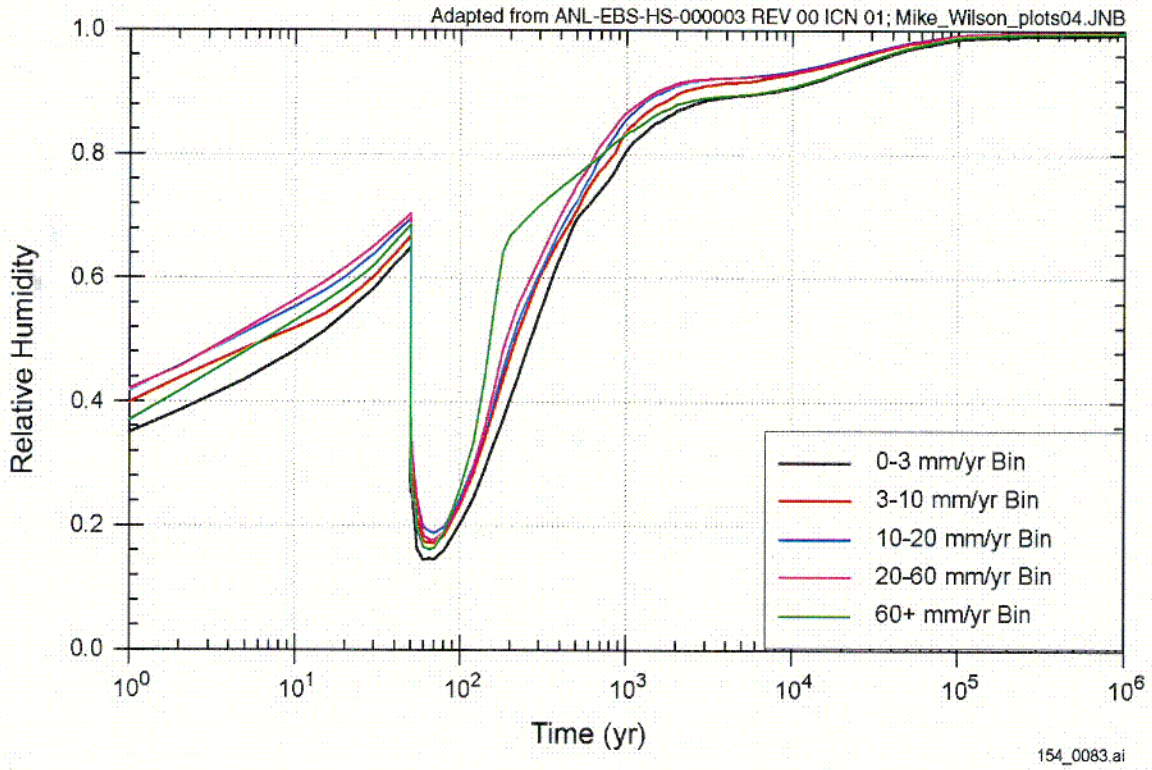

154_0083.ai

Source: CRWMS M&O 2000 [DIRS 153246], Figure 3.3-10.

NOTE: Relative humidity histories averaged into infiltration-level bins. Data for medium overall infiltration into the mountain.

Figure 5.2-5. Waste Package Relative Humidity Histories

C05

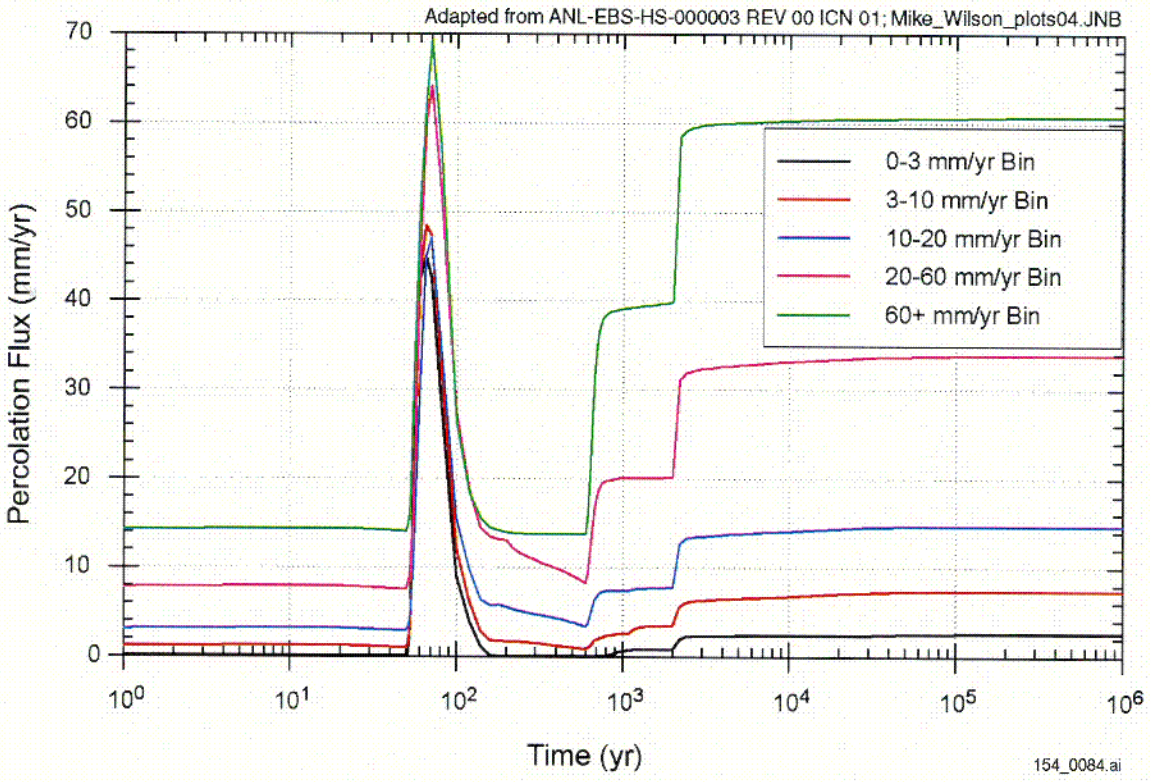

154_0084.ai

Source: CRWMS M&O 2000 [DIRS 153246], Figure 3.3-11.

NOTE: Percolation flux histories averaged into infiltration-level bins. Data for medium overall infiltration into the mountain.

Figure 5.2-6. Histories of Percolation Flux 5 m Above the Drift Crown

C06

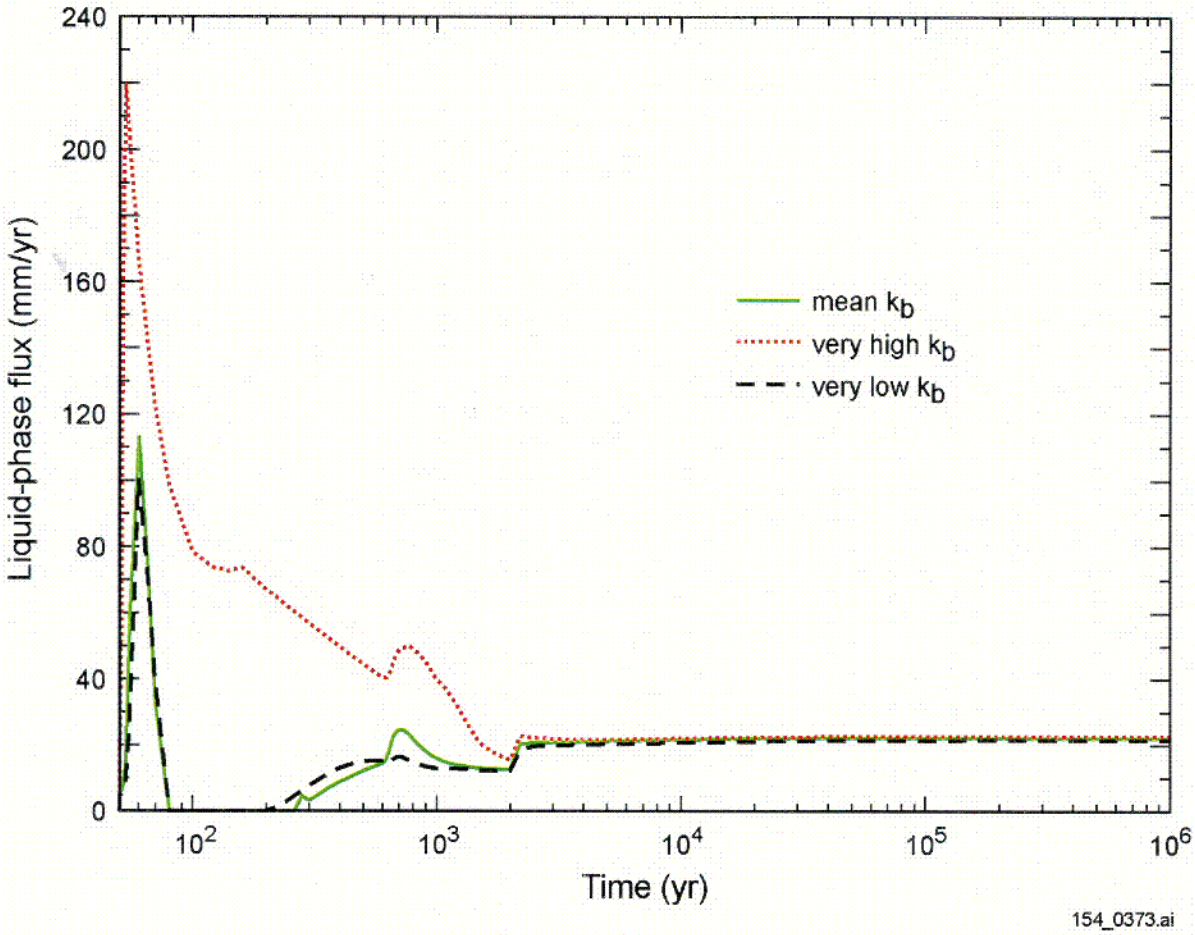

154_0373.ai

Source: Produced using files from Buscheck 2001 [DIRS 155012].

NOTE: Results for a central location in the potential repository. k_b = bulk permeability.

Figure 5.3.1.4.4-1. Liquid Phase Flux 5 m above Drift Wall as a Function of Permeability for the Higher-Temperature Operating Mode

C07

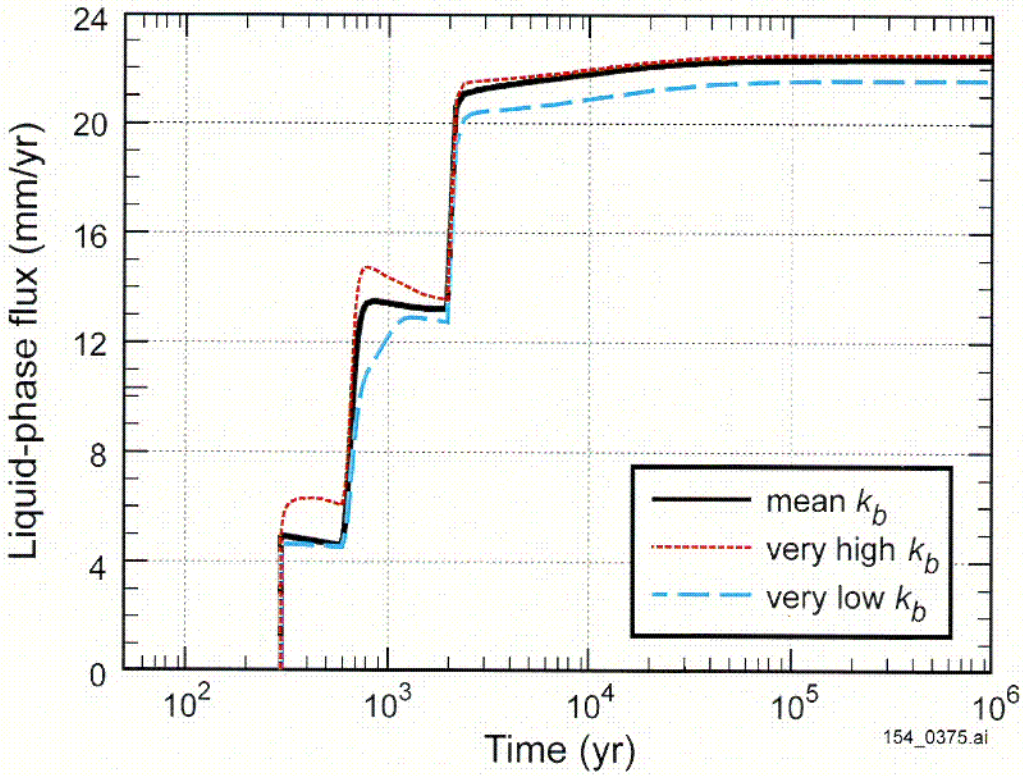

154_0375.ai

Source: Produced using files from Buscheck 2001 [DIRS 155012].

NOTE: Results for a central location in the potential repository. k_b = bulk permeability.

Figure 5.3.1.4.4-2. Postclosure Liquid Phase Flux 5 m above Drift Wall as a Function of Permeability for the Lower-Temperature Operating Mode

C08

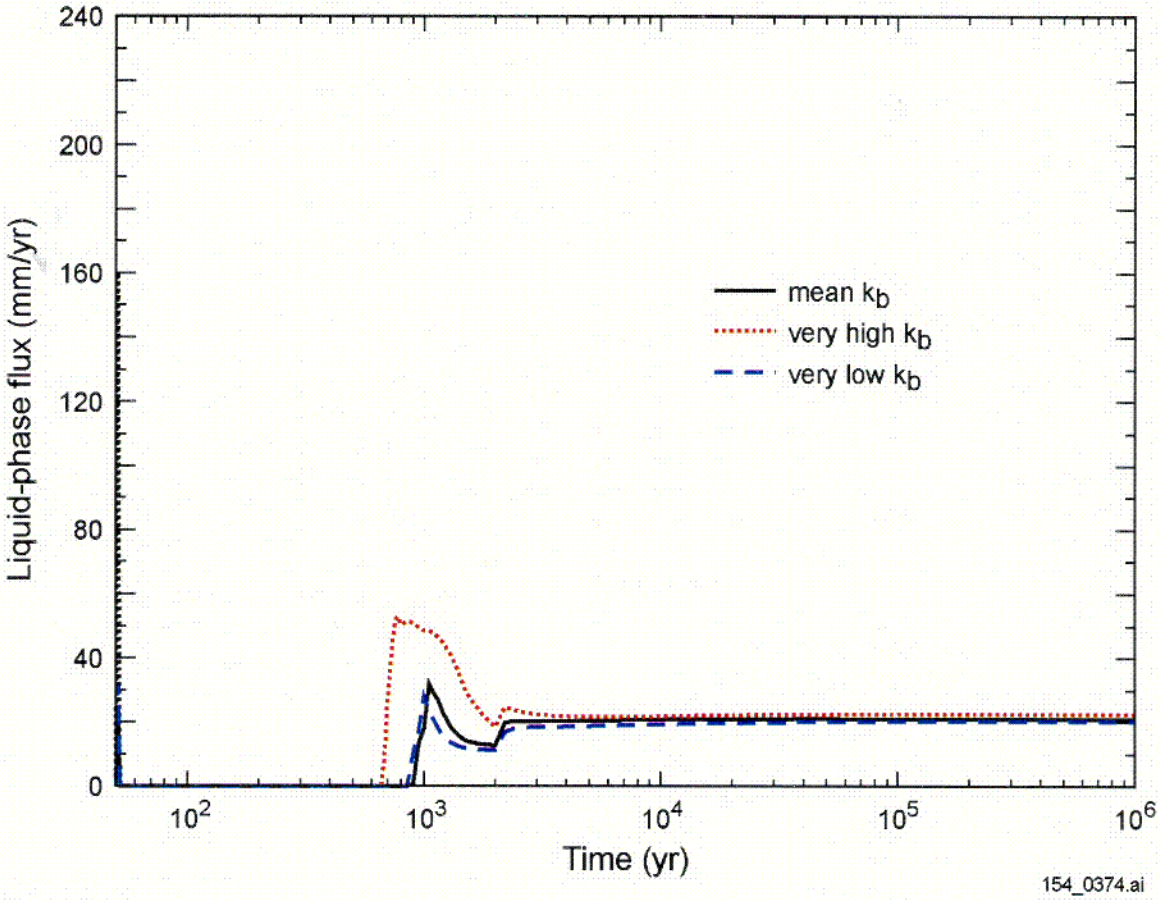

qliq_55_ALLkb

154_0374.ai

Source: Produced using files from Buscheck 2001 [DIRS 155012].

NOTE: Results for a central location in the potential repository. k_b = bulk permeability.

Figure 5.3.1.4.4-3. Liquid Phase Flux 1 m above Drift Wall as a Function of Permeability for the Higher-Temperature Operating Mode

C09

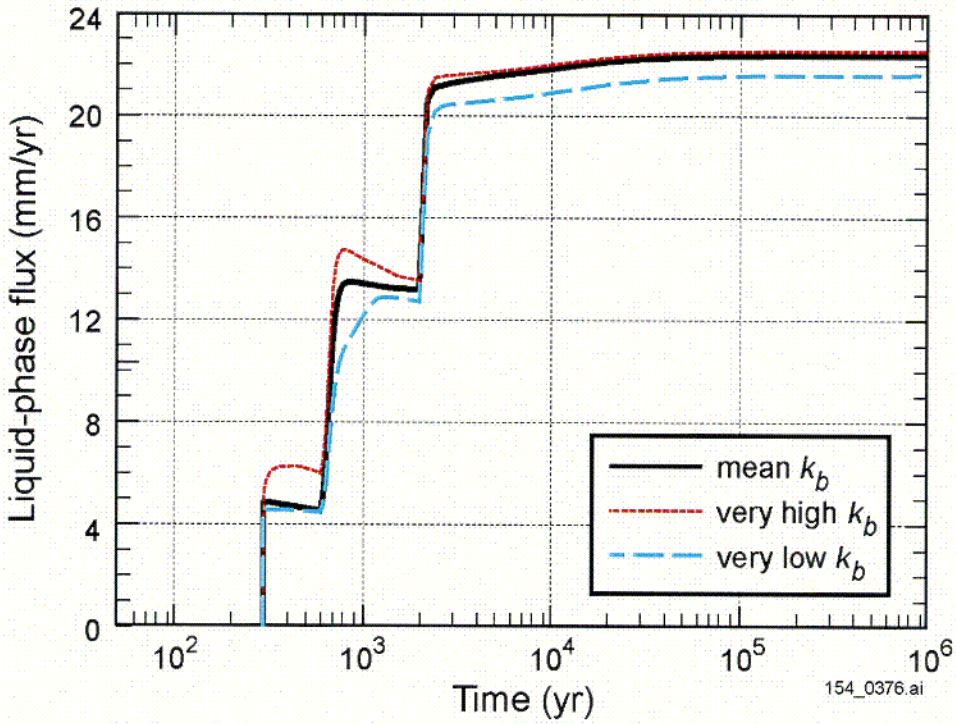

154_0376.ai

Source: Produced using files from Buscheck 2001 [DIRS 155012].

NOTE: Results for a central location in the potential repository. k_b = bulk permeability.

Figure 5.3.1.4.4-4. Postclosure Liquid Phase Flux 1 m above Drift Wall as a Function of Permeability for the Lower-Temperature Operating Mode

C10

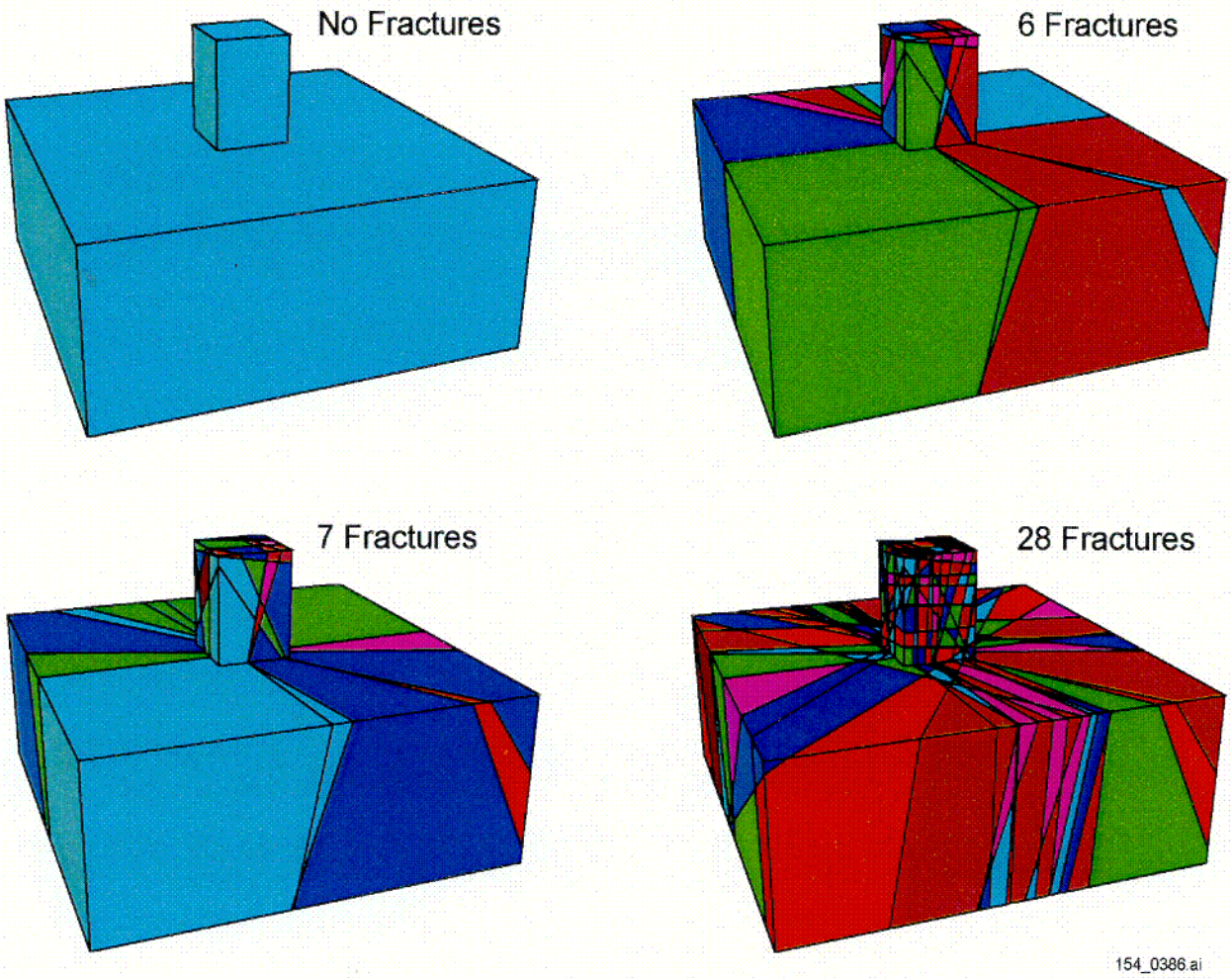

154_0386.ai

Source: Produced using files from Blair 2001 [DIRS 155309].

Figure 5.3.1.4.6-1. Simulations of the Large Block Test

C11

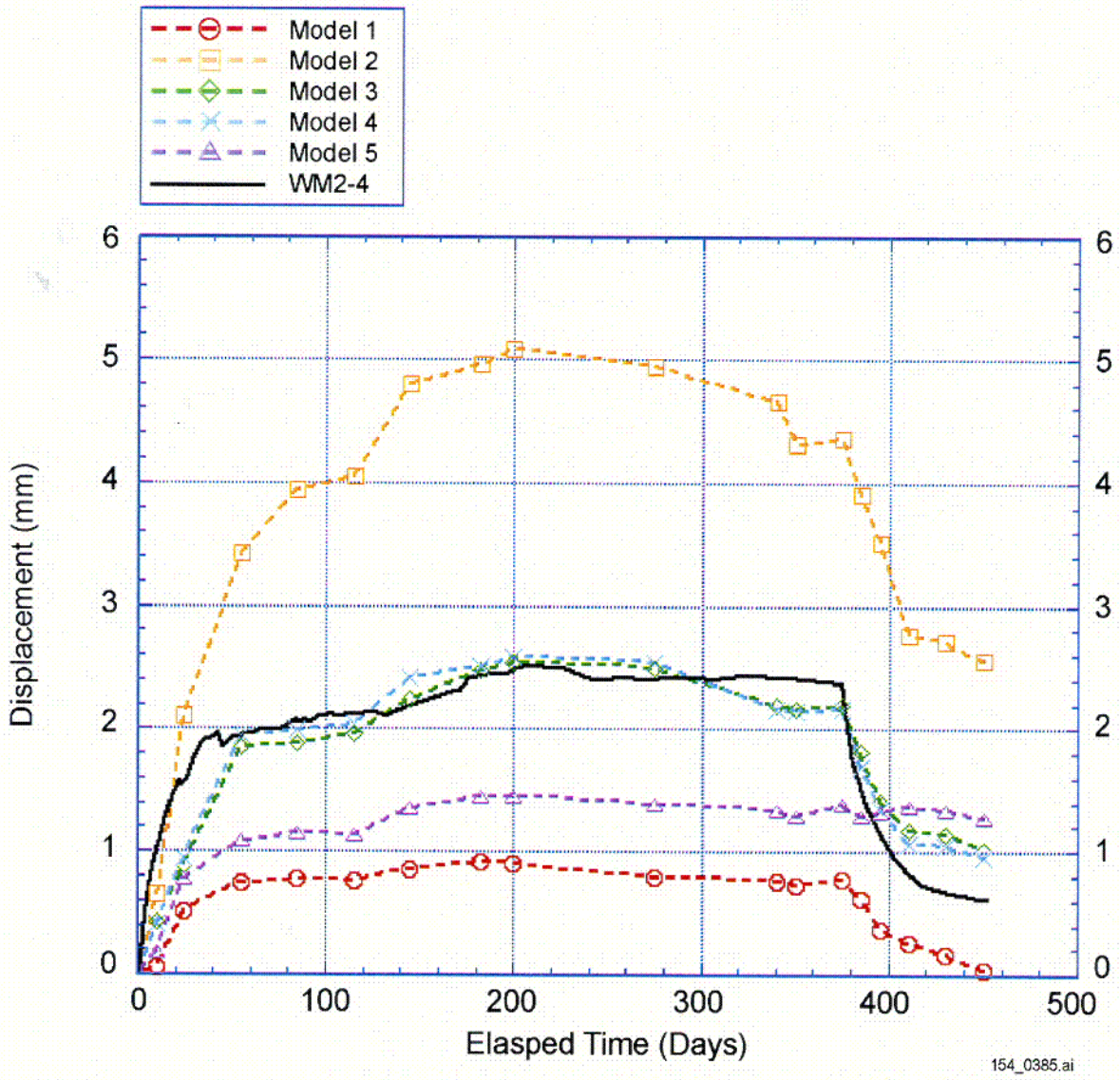

154_0385.ai

Source: Produced using files from Blair 2001 [DIRS 155309].

NOTE: Simulated (dashed lines) and observed (solid line) deformation data.

Figure 5.3.1.4.6-2. Comparison of Simulated and Observed Deformation for Borehole WM-2 in the Large Block Test

C12

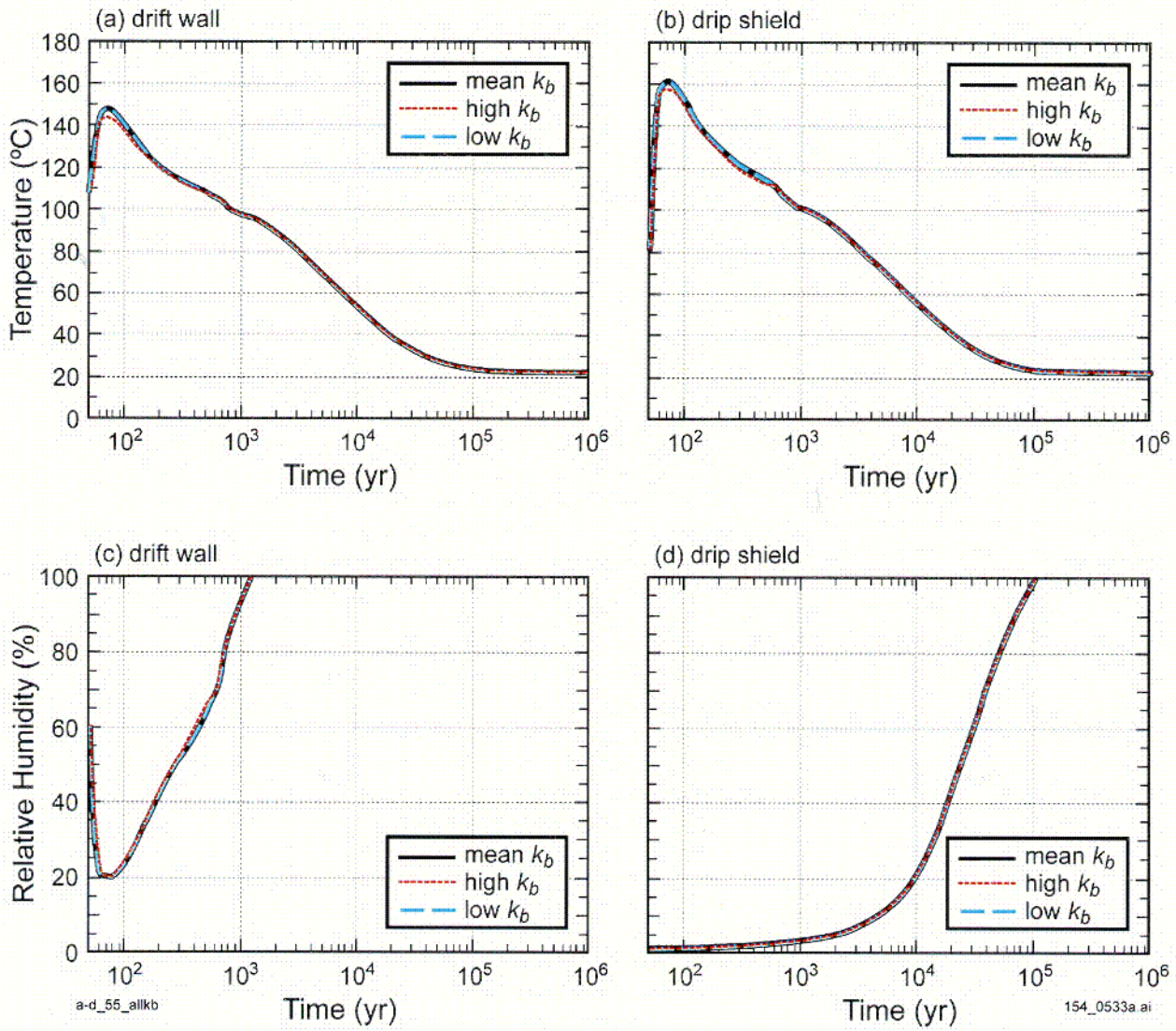

154_0533a.ai

Source: Produced using files from Buscheck 2001 [DIRS 155012].

NOTE: Higher-temperature operating mode drift wall and drip shield temperatures and relative humidities at the central repository location (Location L5C3) as a function of bulk permeability (k_b) for the mean infiltration-flux scenario.

Figure 5.3.1.4.7-1. Drift Wall and Drip Shield Temperatures and Relative Humidities as a Function of Bulk Permeability for the Higher-Temperature Operating Mode (Page 1 of 2)

C13

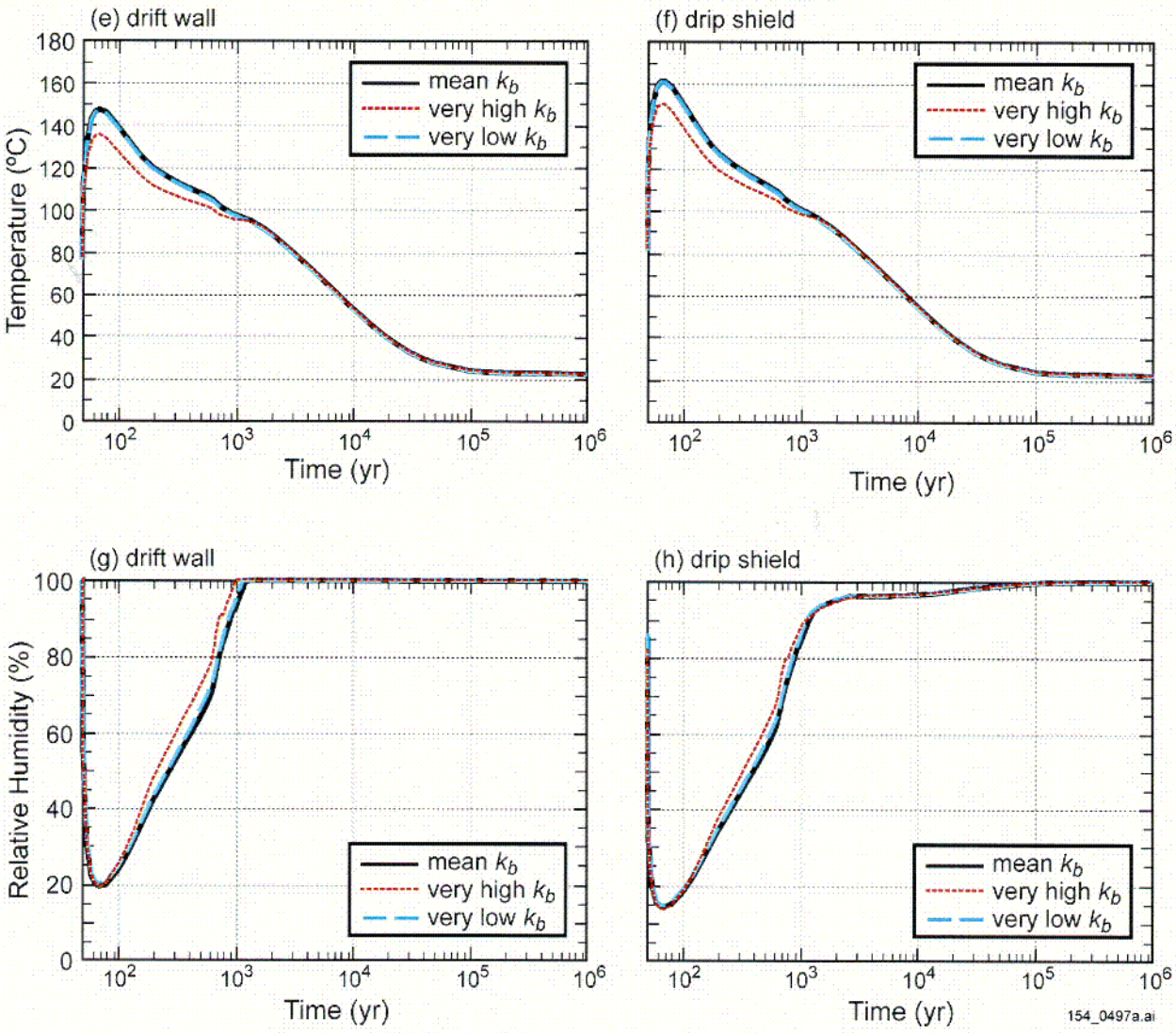

154_0497a.ai

Source: Produced using files from Buscheck 2001 [DIRS 155012].

NOTE: Higher-temperature operating mode drift wall and drip shield temperatures and relative humidities at the central repository location (Location L5C3) as a function of bulk permeability (k_b) for the mean infiltration-flux scenario.

Figure 5.3.1.4.7-1. Drift Wall and Drip Shield Temperatures and Relative Humidities as a Function of Bulk Permeability for the Higher-Temperature Operating Mode (Page 2 of 2)

C14

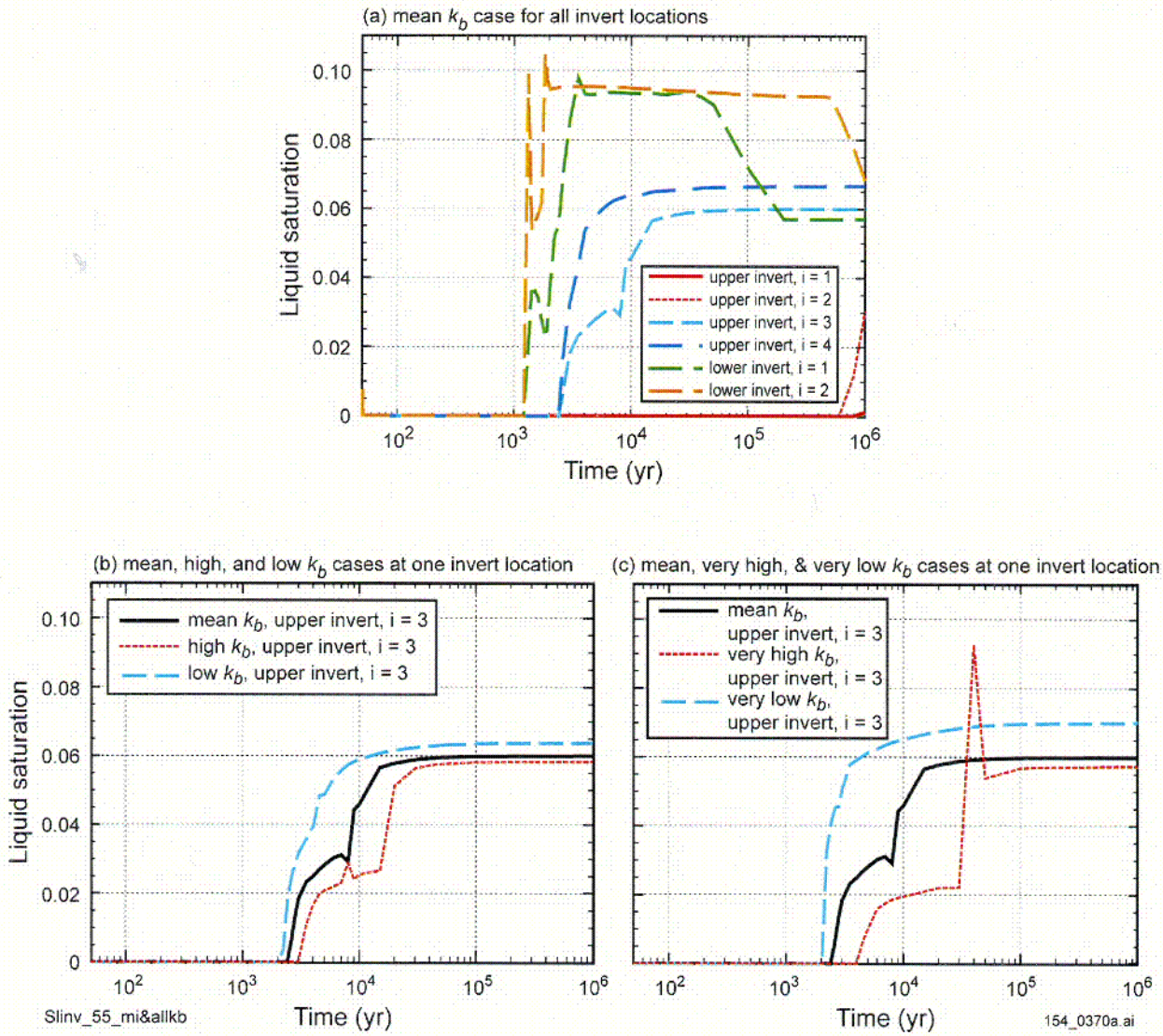

154_0370a.ai

Source: Produced using files from Buscheck 2001 [DIRS 155012].

NOTE: Higher-temperature operating mode invert liquid saturations at the central repository location (Location L5C3) as a function of bulk permeability (k_b) for the mean infiltration-flux scenario.

Figure 5.3.1.4.7-2. Invert Liquid Saturations as a Function of Bulk-Permeability for the Higher-Temperature Operating Mode

C15

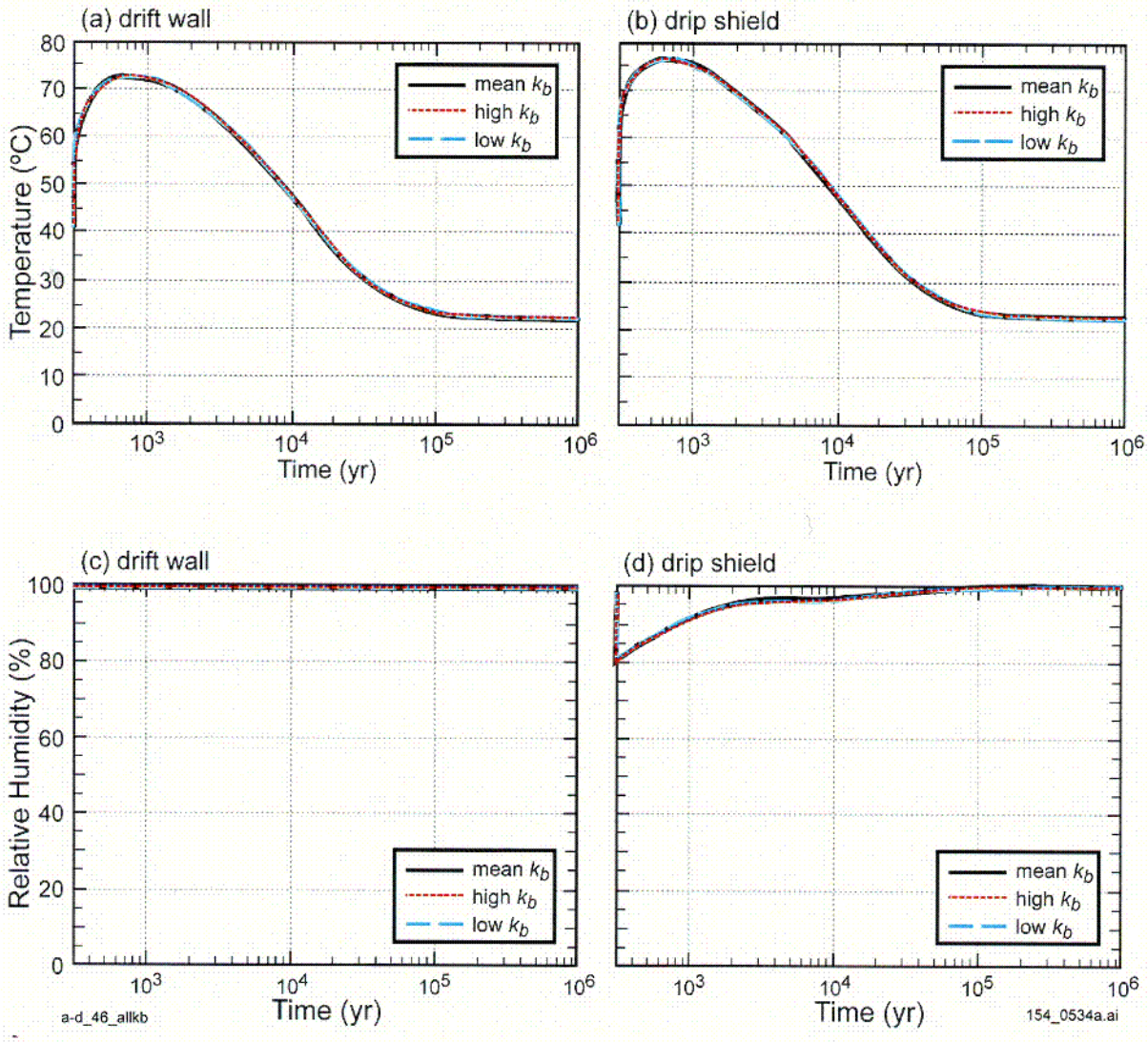

154_0534a.ai

Source: Produced using files from Buscheck 2001 [DIRS 155012].

Figure 5.3.1.4.7-3. Drift Wall and Drip Shield Temperatures and Relative Humidities as a Function of Bulk Permeability for the Lower-Temperature Operating Mode (Page 1 of 2)

C16

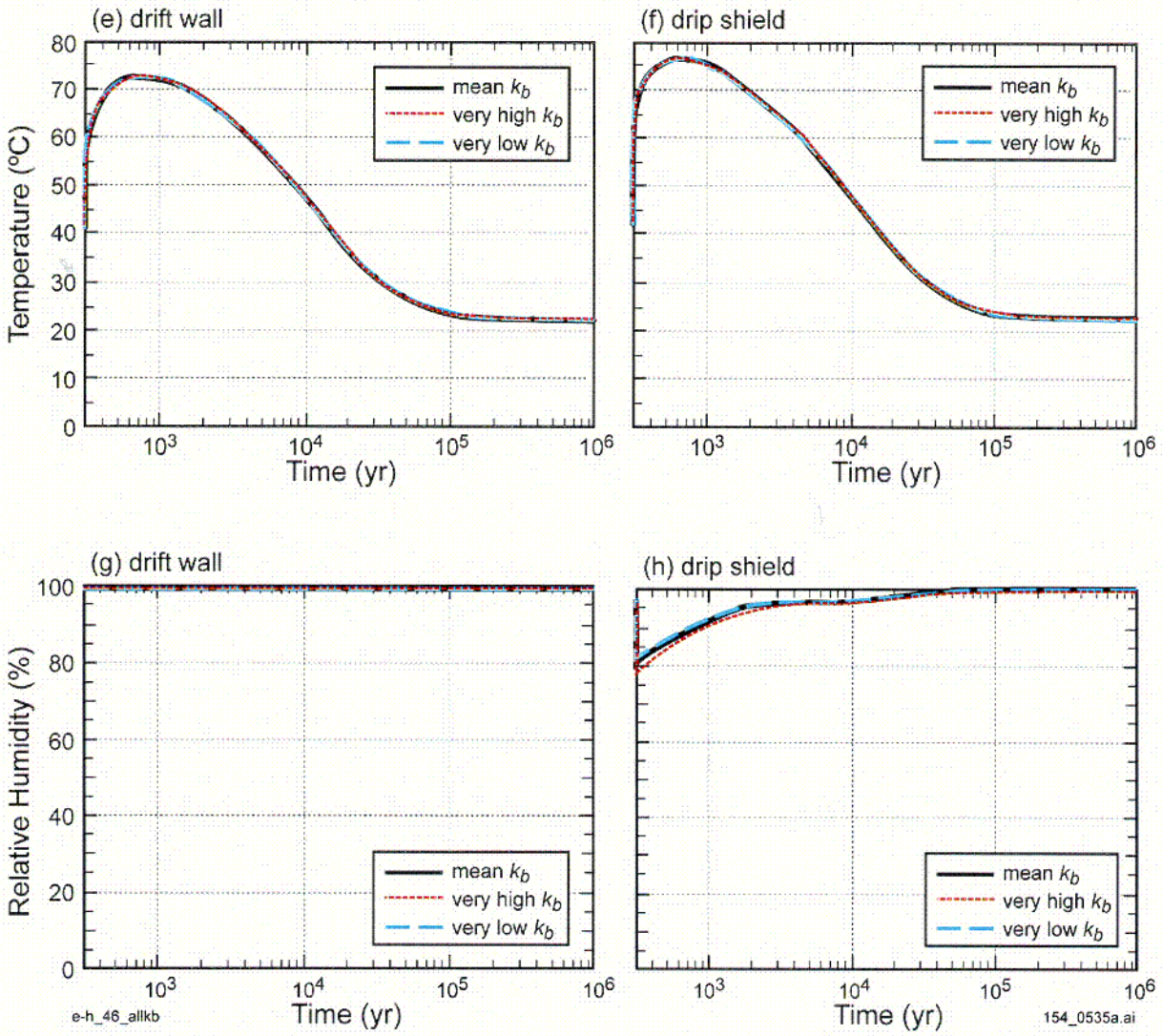

154_0535a.ai

Source: Produced using files from Buscheck 2001 [DIRS 155012].

NOTE: Lower-temperature operating mode drift wall and drip shield temperatures and relative humidities at the central repository location (Location L5C3) as a function of bulk permeability (k_b) for the mean infiltration-flux scenario.

Figure 5.3.1.4.7-3. Drift Wall and Drip Shield Temperatures and Relative Humidities as a Function of Bulk Permeability for the Lower-Temperature Operating Mode (Page 2 of 2)

C17

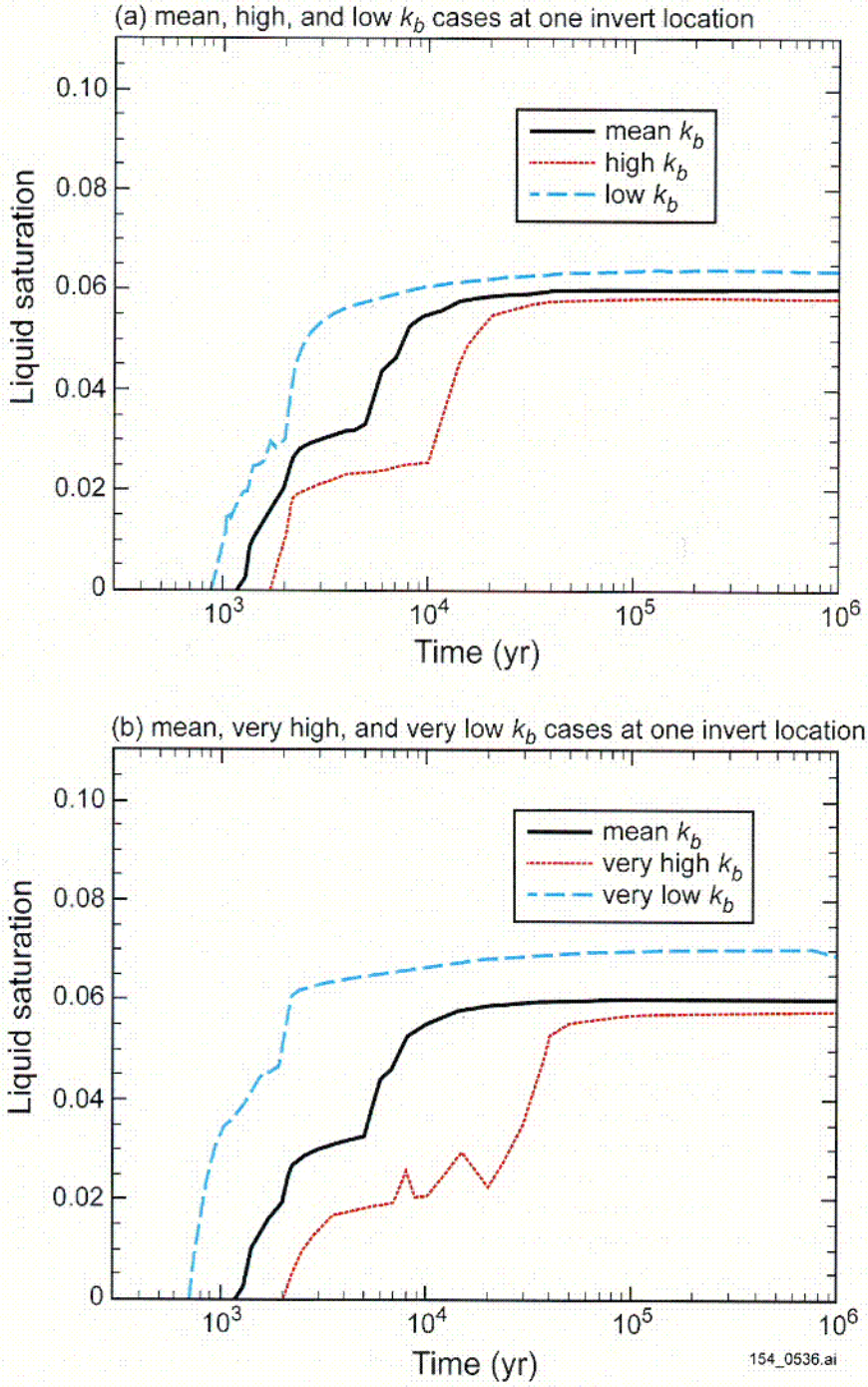

154_0536.ai

Source: Produced using files from Buscheck 2001 [DIRS 155012].

NOTE: Lower-temperature operating mode invert liquid saturations at the central repository location (Location L5C3) as a function of bulk permeability (k_b) for the mean infiltration-flux scenario.

Figure 5.3.1.4.7-4. Invert Liquid-Saturations as a Function of Bulk Permeability for the Lower-Temperature Operating Mode

C18

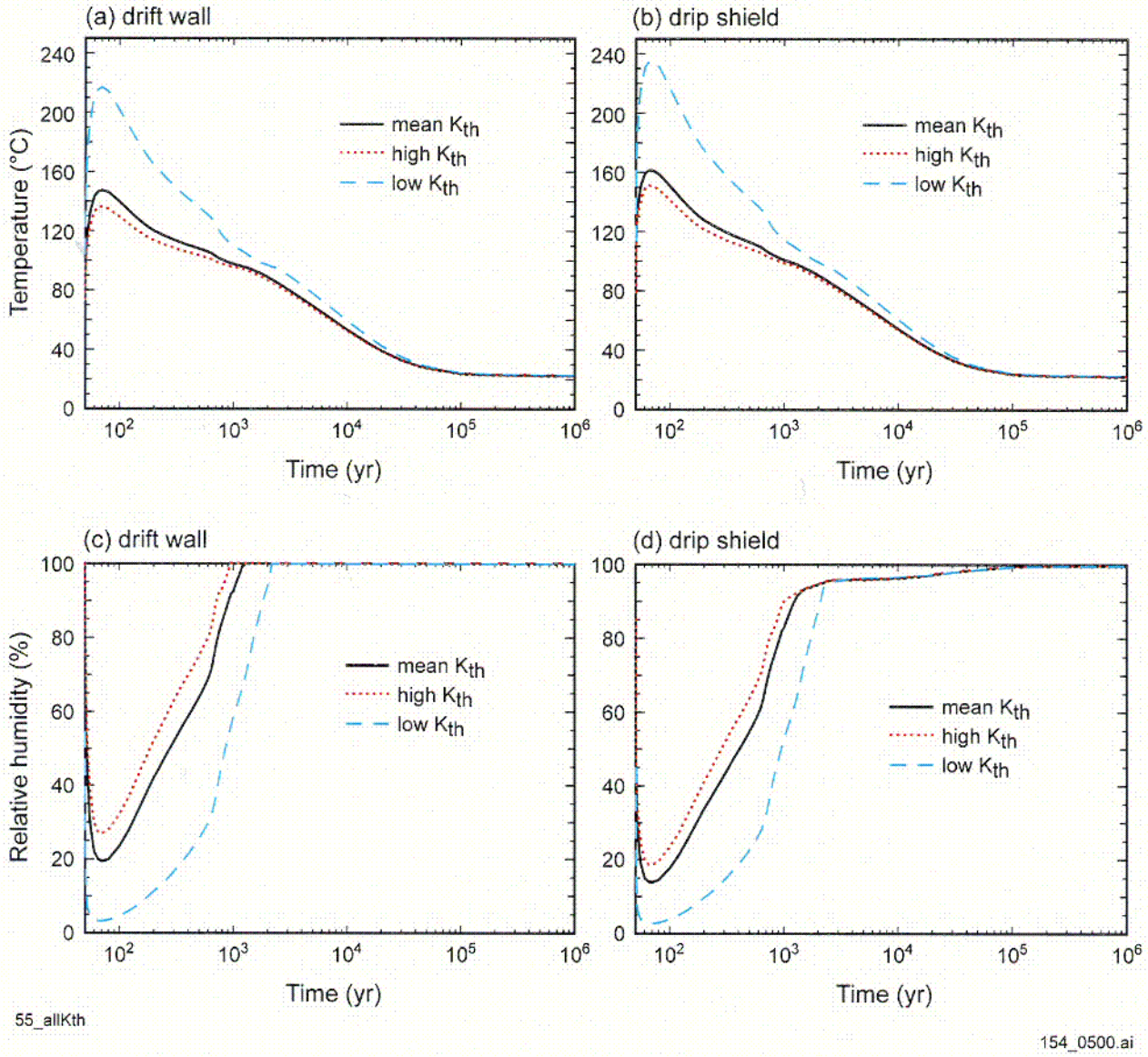

154_0500.ai

Source: Produced using files from Buscheck 2001 [DIRS 155012].

Figure 5.3.1.4.8-1. Temperature and Relative Humidity at the Drift Wall and Drip Shield as a Function of Host-Rock Thermal Conductivity for the Central Repository (L5C3) Location of the Higher-Temperature Operating Mode and the Mean Infiltration-Flux Scenario

C19

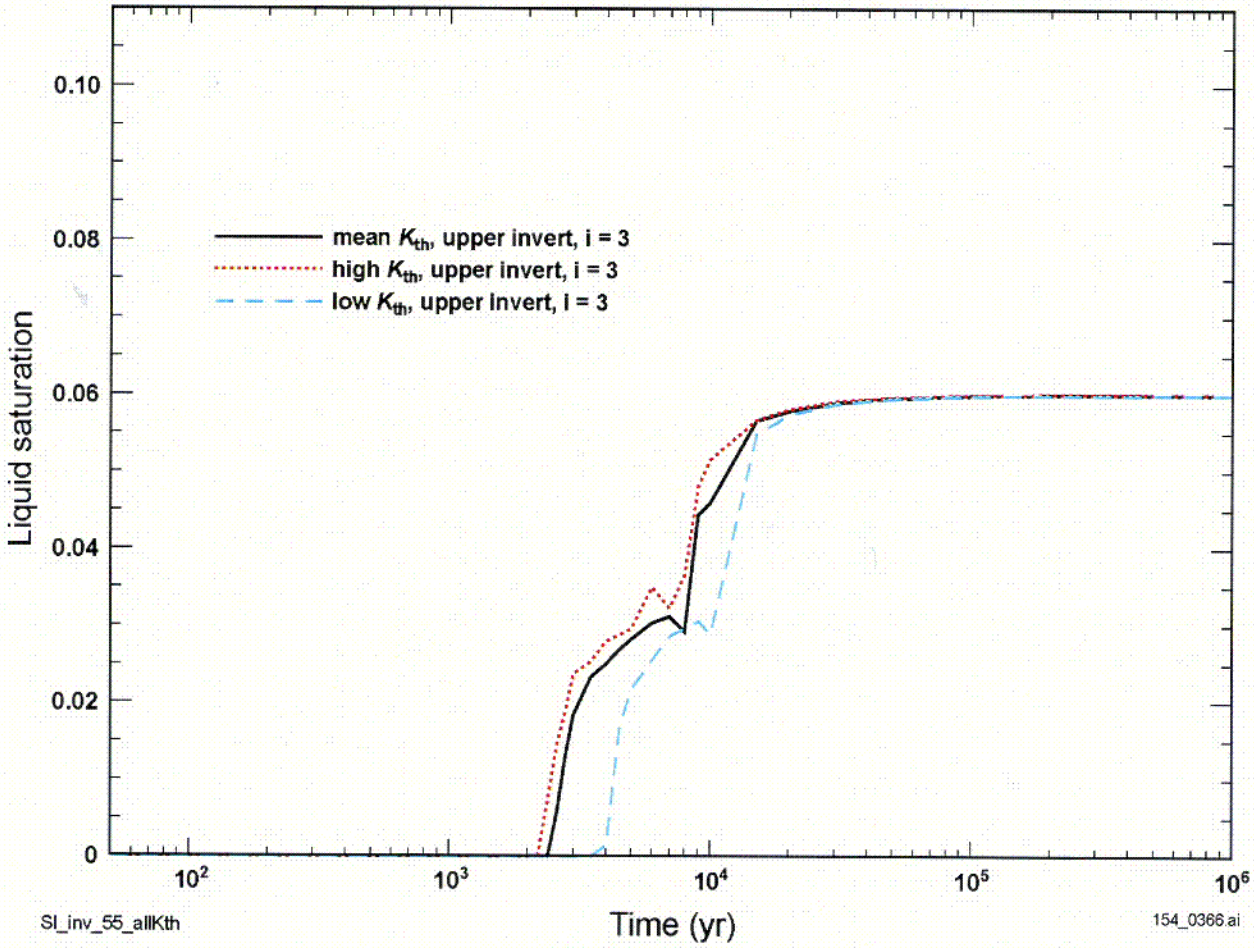

154_0366.ai

Source: Produced using files from Buscheck 2001 [DIRS 155012].

Figure 5.3.1.4.8-2. Liquid-Saturation in the Invert as a Function of Host-Rock Thermal Conductivity for the Central Repository (L5C3) Location of the Higher-Temperature Operating Mode and the Mean Infiltration-Flux Scenario

C20

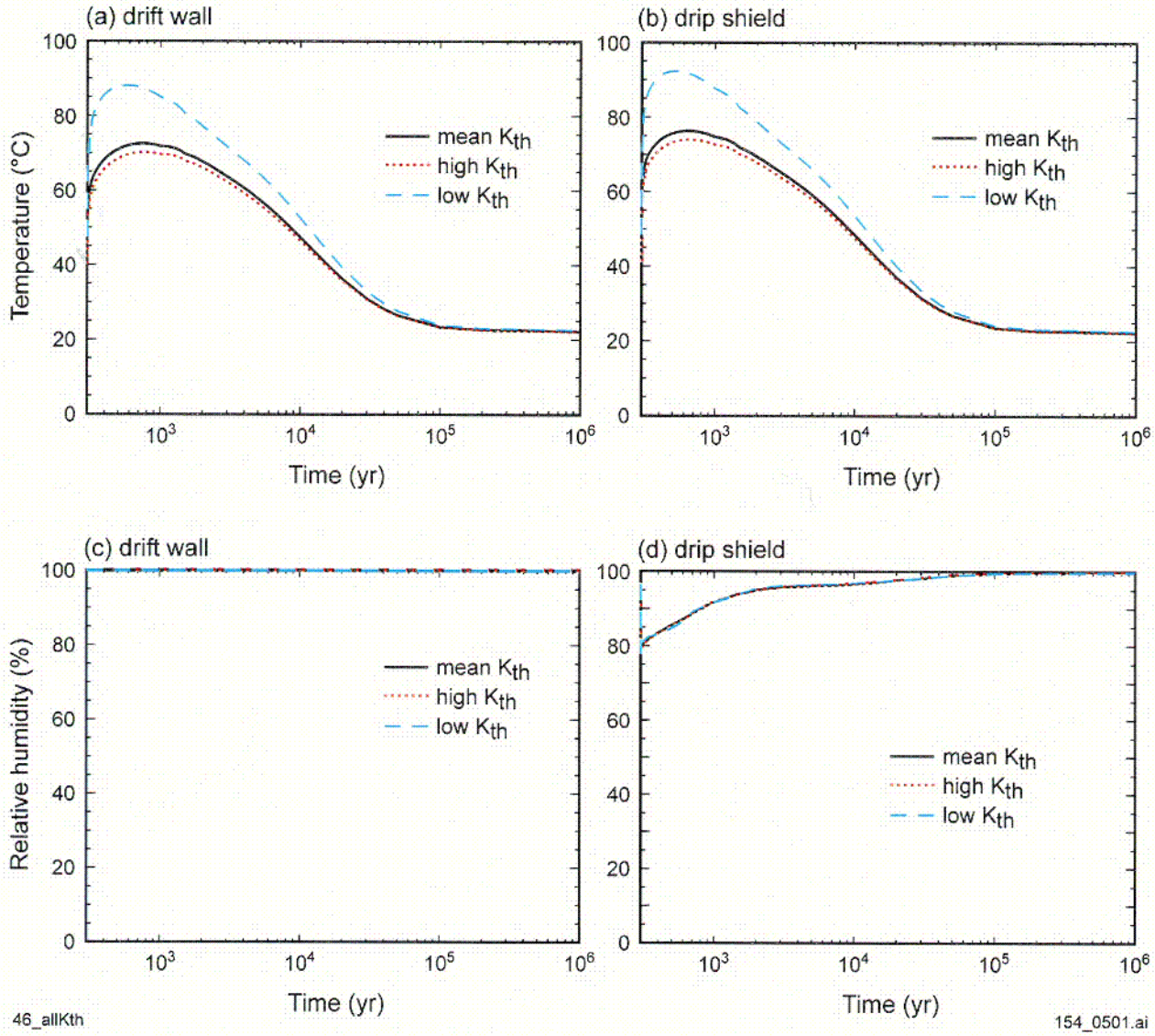

Source: Produced using files from Buscheck 2001 [DIRS 155012].

Figure 5.3.1.4.8-3. Temperature and Relative Humidity at the Drift Wall and Drip Shield as a Function of Host-Rock Thermal Conductivity for the Central Repository (L5C3) Location of the Lower-Temperature Operating Mode and the Mean Infiltration-Flux Scenario

C21

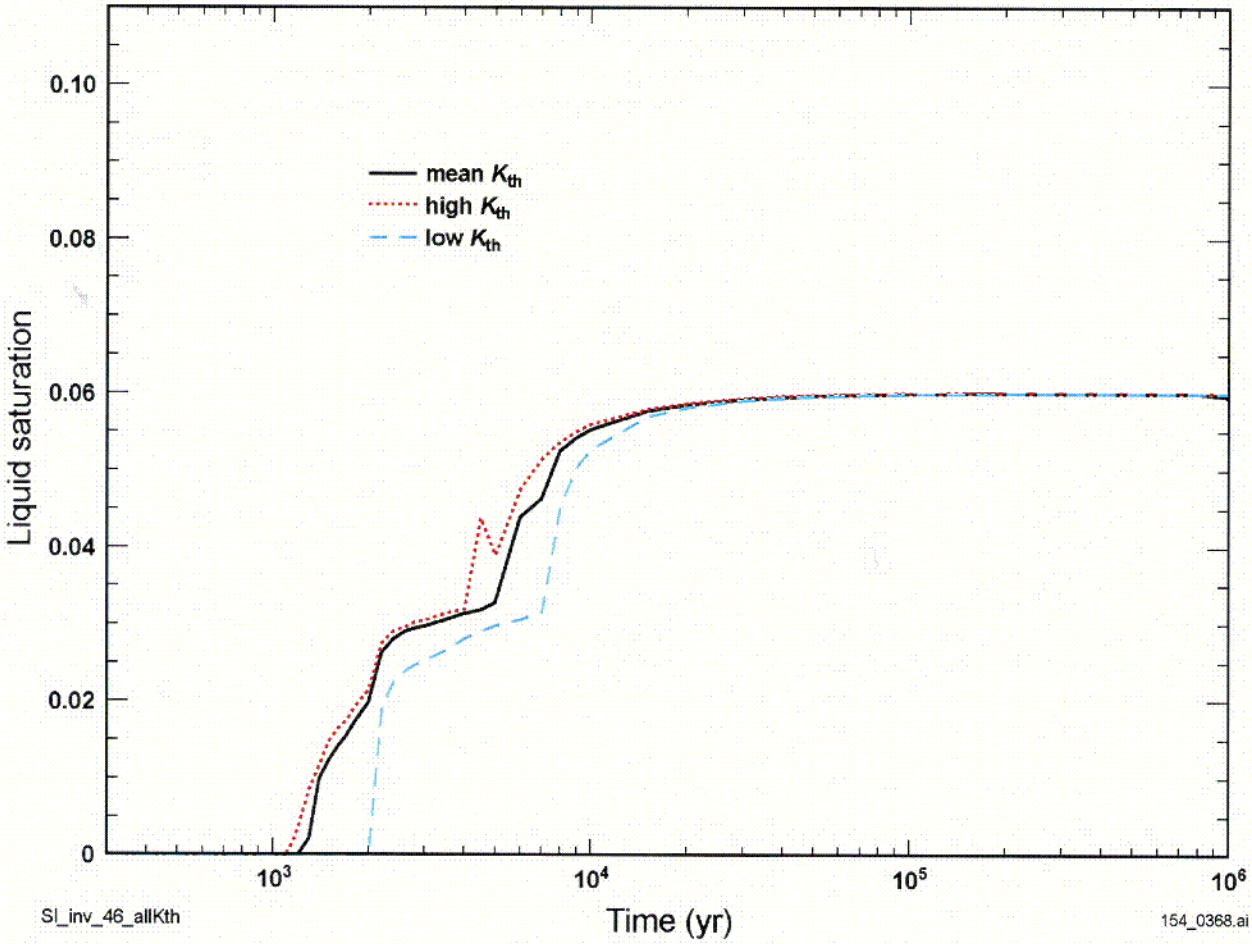

154_0368.ai

Source: Produced using files from Buscheck 2001 [DIRS 155012].

Figure 5.3.1.4.8-4. Liquid-saturation in the Invert as a Function of Host-Rock Thermal Conductivity for the Central Repository (L5C3) Location of the Lower-Temperature Operating Mode and the Mean Infiltration-Flux Scenario

C22

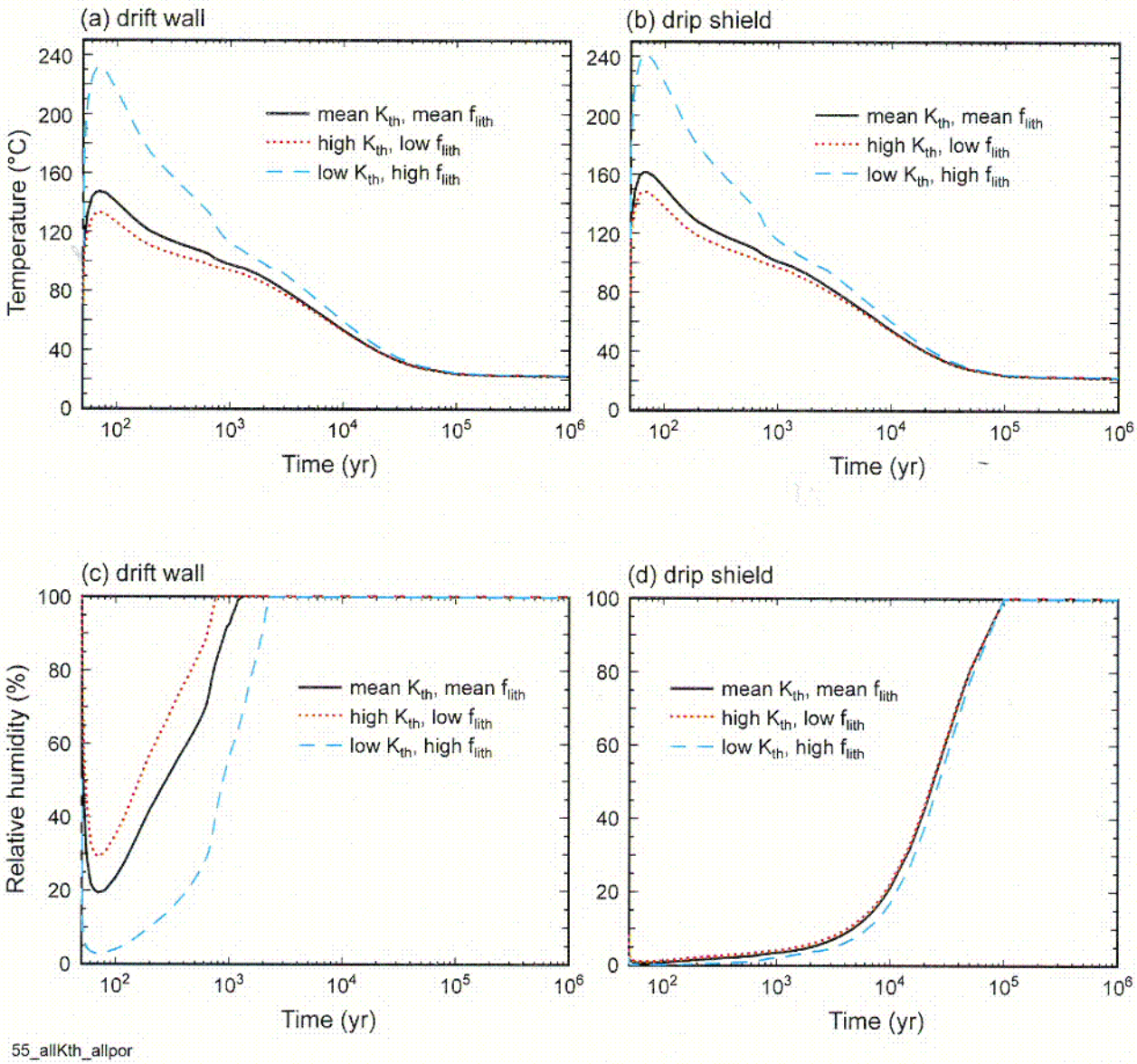

154_0364.ai

Source: Produced using files from Buscheck 2001 [DIRS 155012].

NOTE: Higher-temperature operating mode, drift wall and drip shield temperature and relative humidity at the central repository location (Location L5C3) as a function of mean, high, and low lithophysal porosity (f_{lith}) associated with appropriate thermal conductivity (K_{th}) for the mean infiltration-flux scenario.

Figure 5.3.1.4.9-1. Higher-Temperature Operating Mode as a Function of Mean, High, and Low Lithophysal Porosity (f_{lith}) for the Mean Infiltration-Flux Scenario

C23

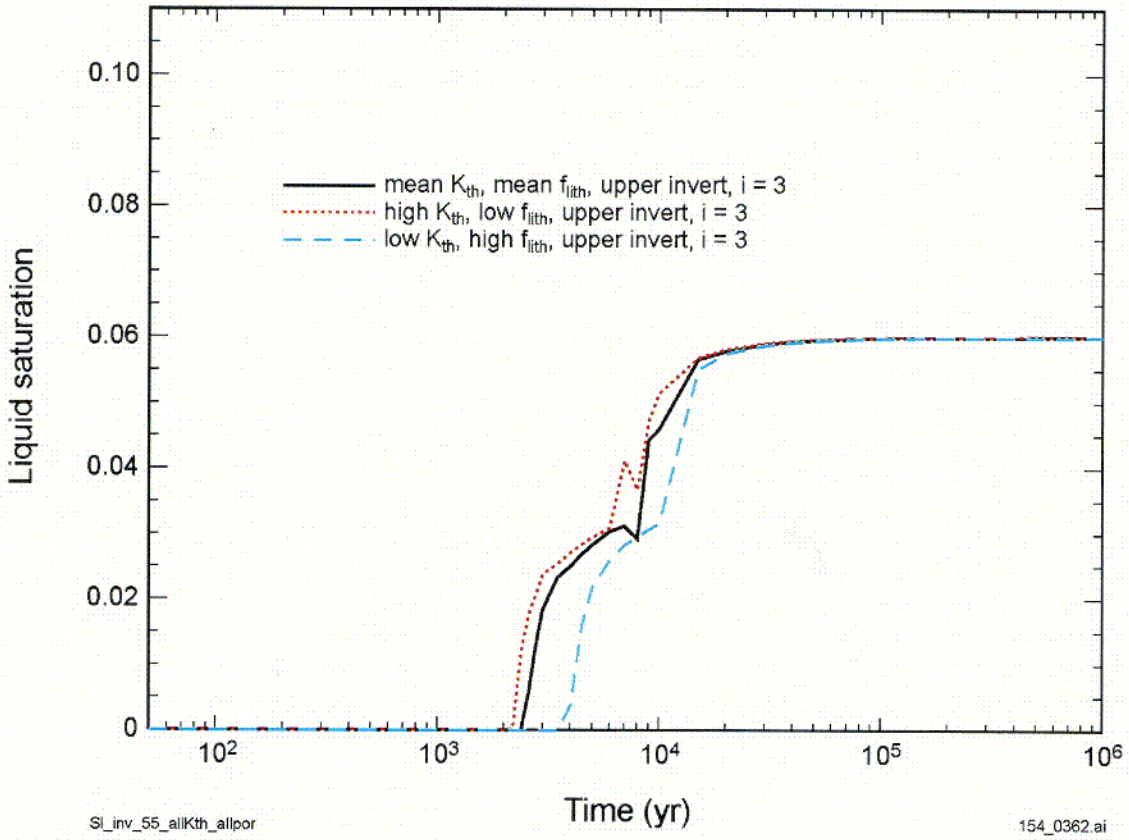

154_0362.ai

Source: Produced using files from Buscheck 2001 [DIRS 155012].

NOTE: Higher-temperature operating mode invert liquid saturations at the central repository location (Location L5C3) as a function of mean, high, and low lithophysal porosity (f_{lith}) associated with appropriate thermal conductivity (K_{th}) for the mean infiltration-flux scenario.

Figure 5.3.1.4.9-2. Higher-Temperature Operating Mode Invert Liquid-Saturations as a Function of Mean, High, and Low Lithophysal Porosity (f_{lith}) for the Mean Infiltration-Flux Scenario

C24

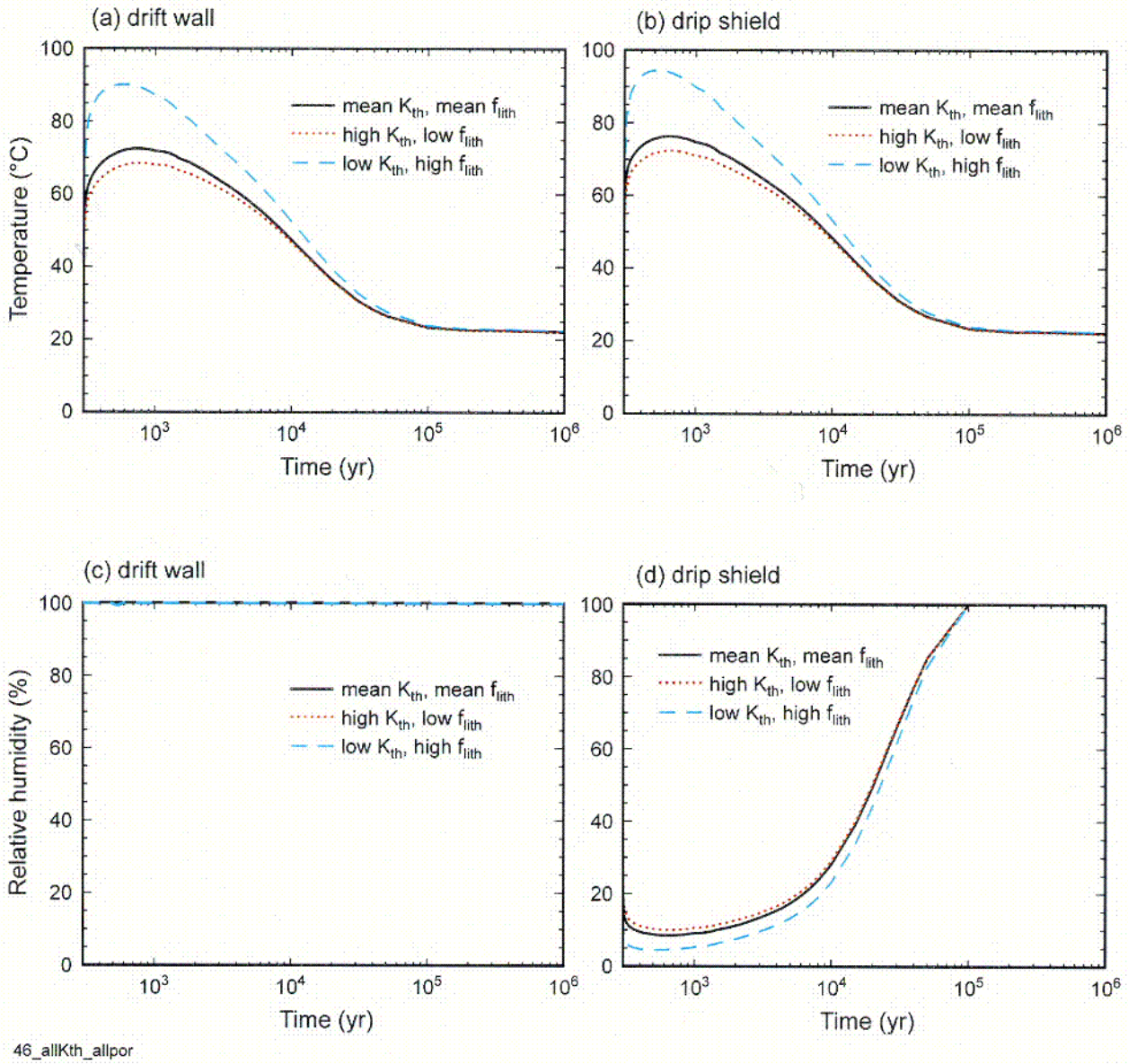

154_0363.ai

Source: Produced using files from Buscheck 2001 [DIRS 155012].

NOTE: Lower-temperature operating mode drift wall and drip shield temperatures and relative humidities at the central repository location (Location L5C3) as a function of mean, high, and low lithophysal porosity (f_{lith}) associated with appropriate thermal conductivity (K_{th}) for the mean infiltration-flux scenario.

Figure 5.3.1.4.9-3. Lower-Temperature Operating Mode Drift Wall and Drip Shield Temperatures and Relative Humidities as a Function of Mean, High, and Low Lithophysal Porosity (f_{lith}) for the Mean Infiltration-Flux Scenario

C25

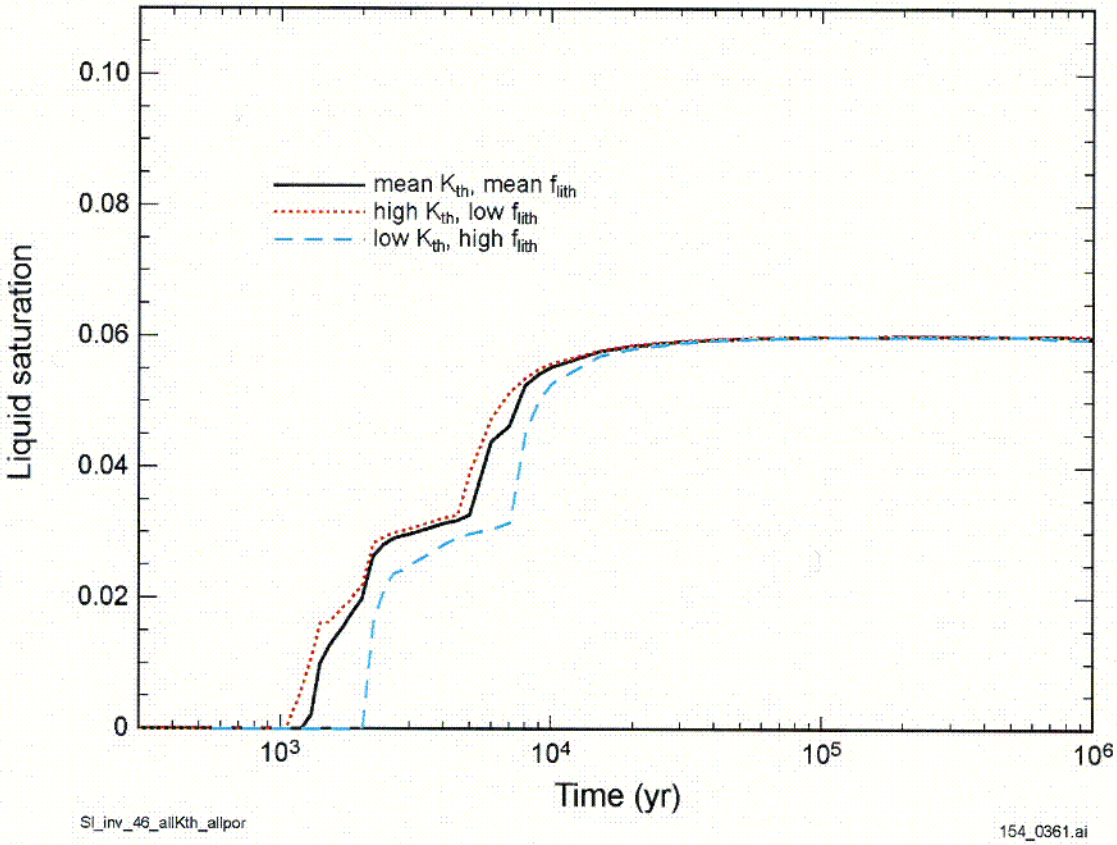

154_0361.ai

Source: Produced using files from Buscheck 2001 [DIRS 155012].

Figure 5.3.1.4.9-4. Lower-Temperature Operating Mode Invert Saturation for the Central Repository Location (Location L5C3) as a Function of Mean, High and Low Lithophysal Porosity (f_{lith}) Associated with Appropriate Thermal Conductivity (K_{th}) for the Mean Infiltration-Flux Scenario

C26

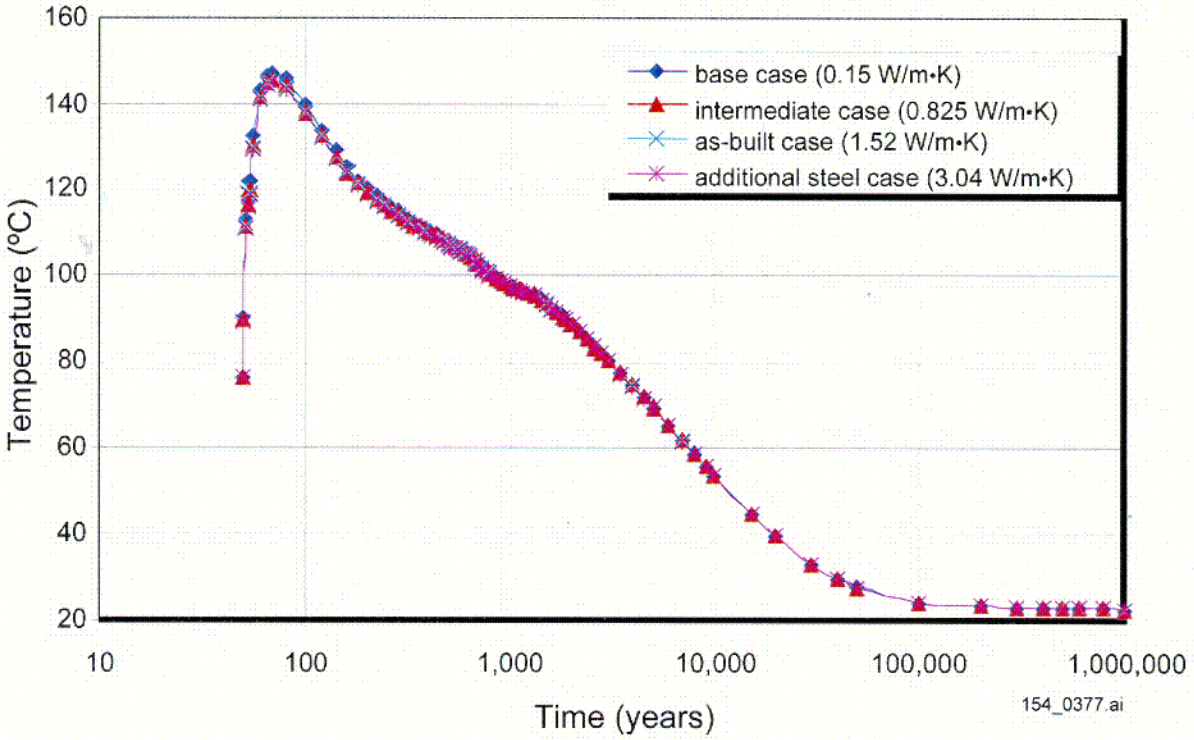

154_0377.ai

Source: Produced using files from Reed 2001 [DIRS 155076].

Figure 5.3.1.4.10-1. Drift Wall (Crown) Temperature Sensitivity to Invert Thermal Conductivity for the Higher-Temperature Operating Mode

C27

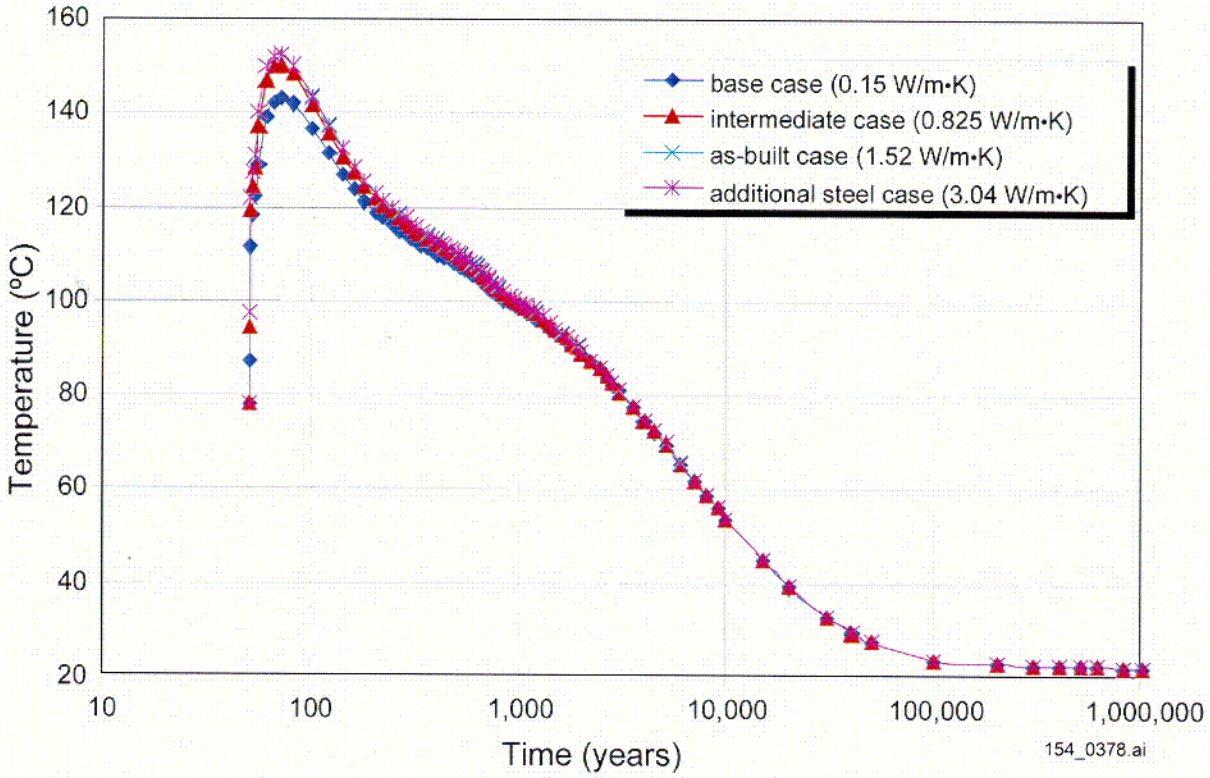

154_0378.ai

Source: Produced using files from Reed 2001 [DIRS 155076].

Figure 5.3.1.4.10-2. Invert (Lower-Center) Temperature Sensitivity to Invert Thermal Conductivity for the Higher-Temperature Operating Mode

C28

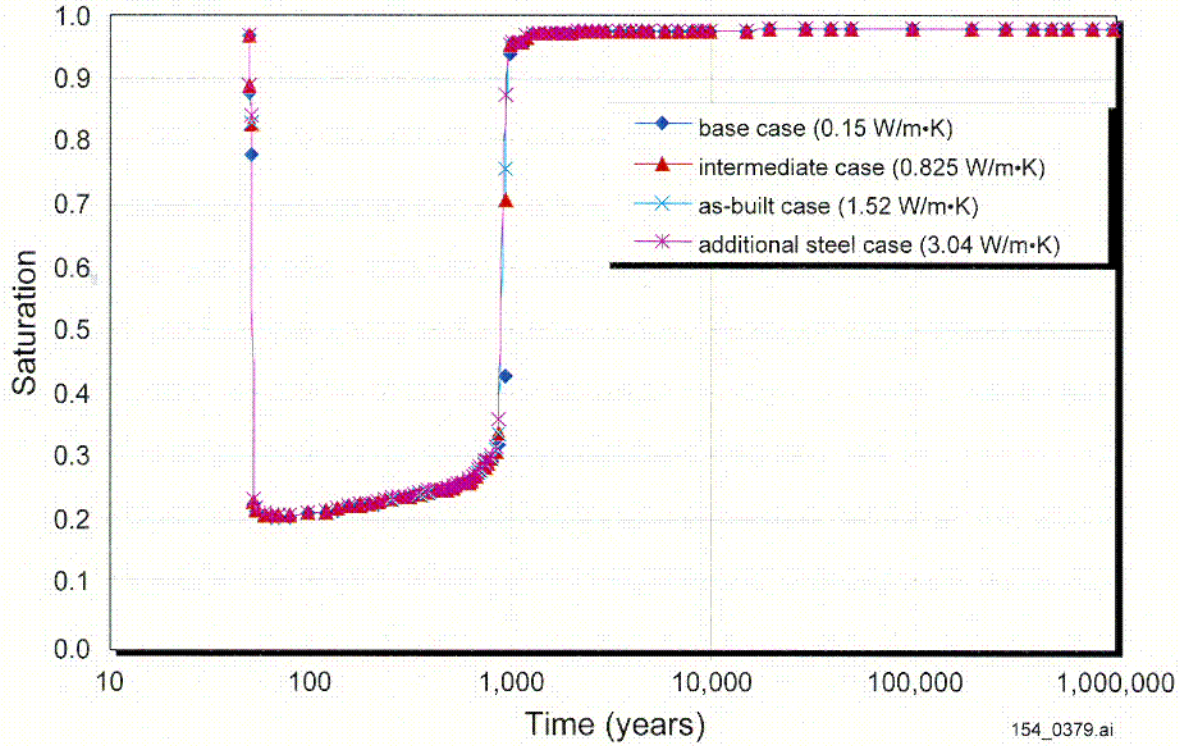

154_0379.ai

Source: Produced using files from Reed 2001 [DIRS 155076].

Figure 5.3.1.4.10-3. Drift Wall (Crown) Liquid Saturation Sensitivity to Invert Thermal Conductivity for the Higher-Temperature Operating Mode

C29

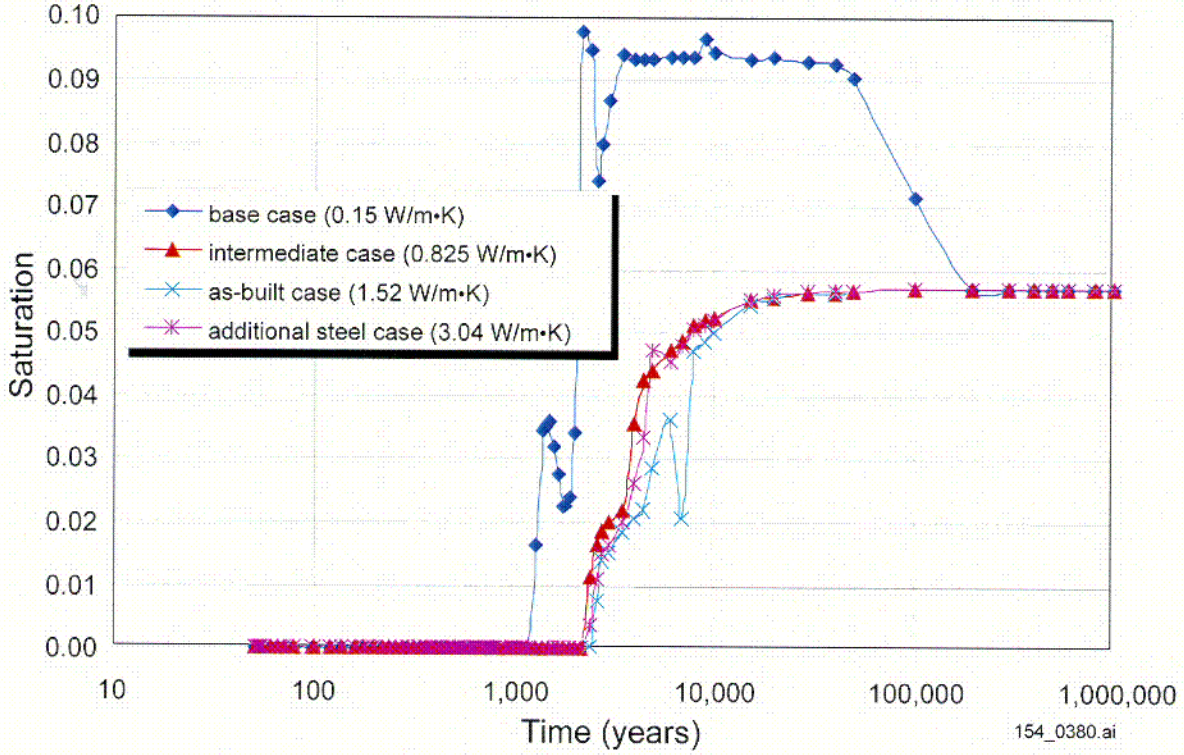

154_0380.ai

Source: Produced using files from Reed 2001 [DIRS 155076].

Figure 5.3.1.4.10-4. Invert (Lower-Center) Liquid Saturation Sensitivity to Invert Thermal Conductivity for the Higher-Temperature Operating Mode

C30

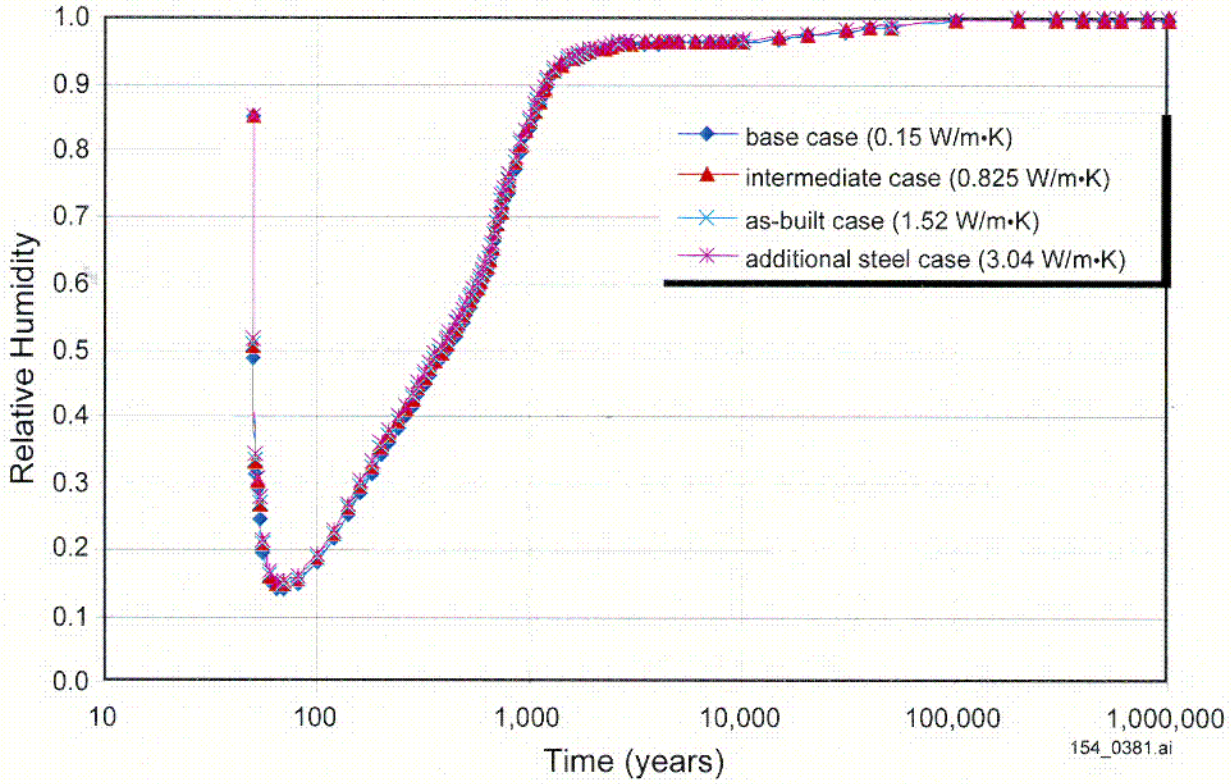

154_0381.ai

Source: Produced using files from Reed 2001 [DIRS 155076].

Figure 5.3.1.4.10-5. Drip Shield (Top) Relative Humidity Sensitivity to Invert Thermal Conductivity for the Higher-Temperature Operating Mode

C31

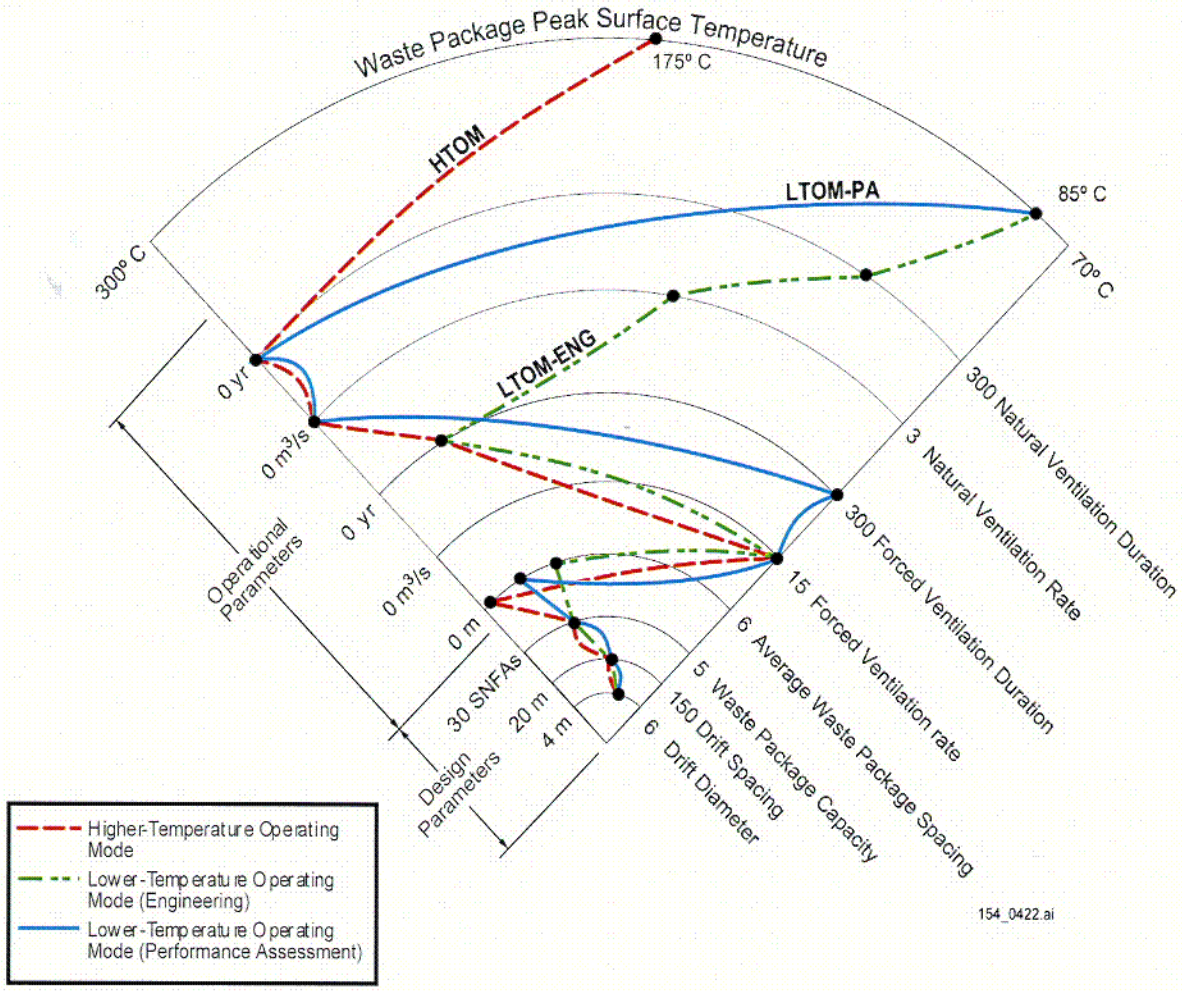

154_0422.ai

Source: Produced from information in BSC 2001 [DIRS 154864] and BSC 2001 [DIRS 155010].

NOTE: Two sets of parameters are shown that can meet the lower-temperature operating mode goal. Black dots represent values of design and operating parameters which, when combined, result in the peak waste package temperatures shown. Lines through the black dots represent three combinations of parameters being evaluated during the SR time period. HTOM = higher-temperature operating mode; PA = performance assessment base case; ENG = engineering evaluations.

Figure 5.3.1.4.11-1. Design and Operating Mode Parameters Used to Meet Peak Waste Package Temperature Goals

C32

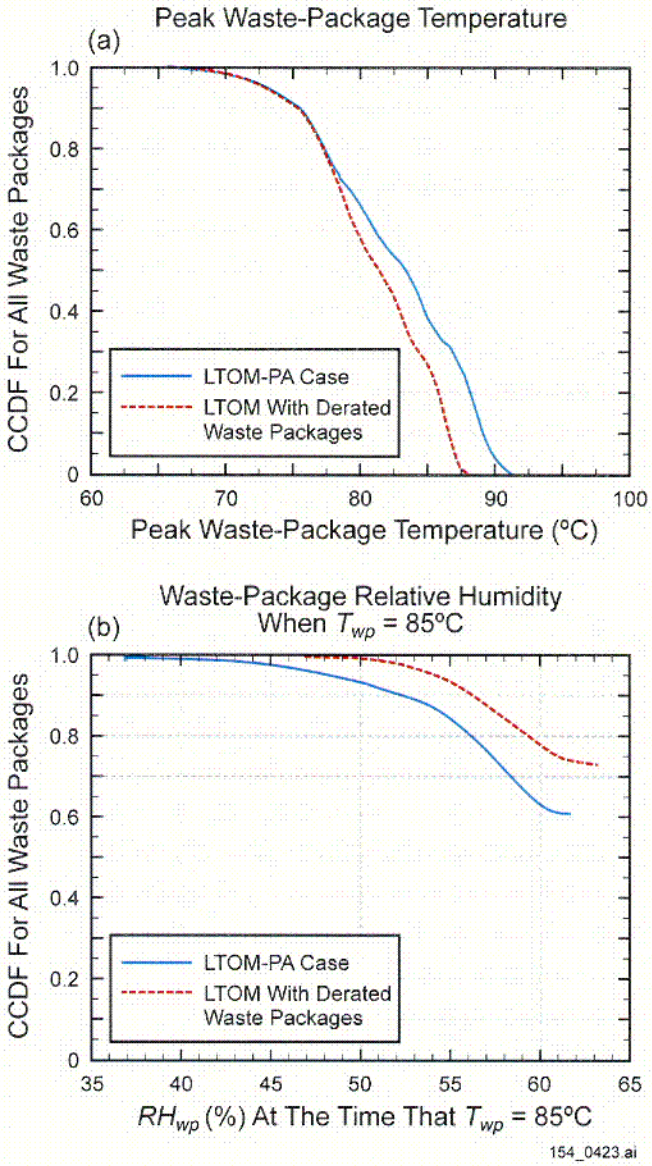

154_0423.ai

Source: Produced using files from Buscheck 2001 [DIRS 155243].

NOTE: Temperature and relative humidity (*RH*) when the waste package temperature (T_{wp}) is 85°C considering repository footprint, infiltration flux map, and variability among waste packages. LTOM-PA = lower-temperature operating mode used in the performance assessment base case. CCDF = complementary cumulative distribution function.

Figure 5.3.1.4.11-2. Waste Package Temperatures and Relative Humidity for Two Methods of Archiving the Lower-Temperature Operating Mode

C33

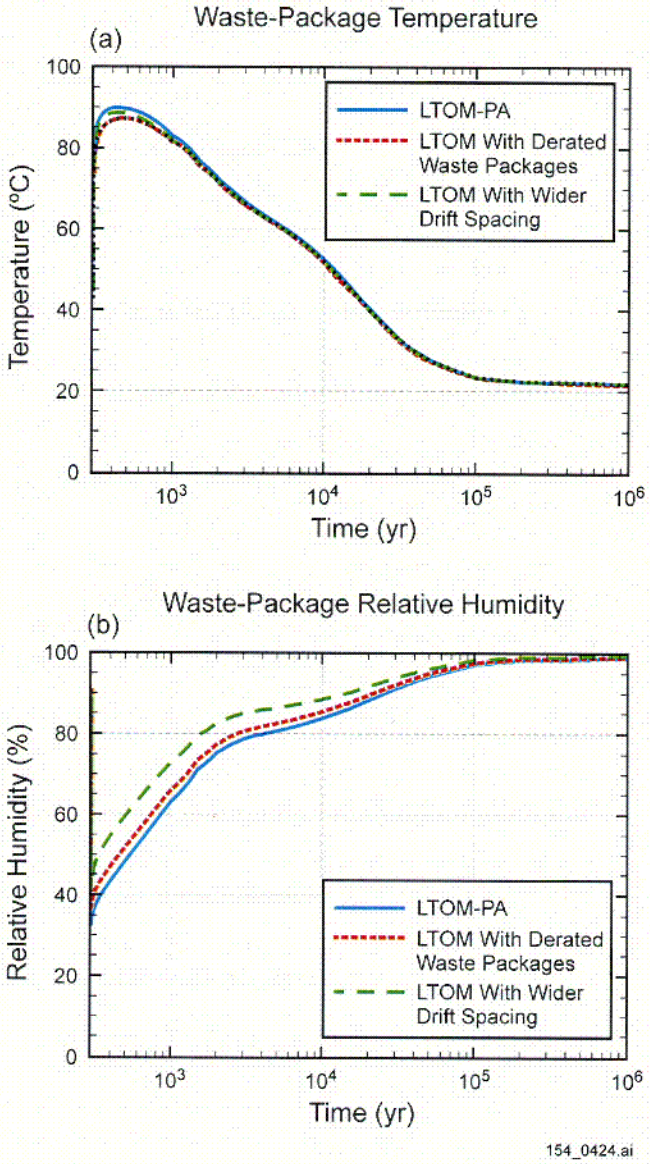

154_0424.ai

Source: Produced using files from Buscheck 2001 [DIRS 155243].

NOTE: Figure depicts three lower-temperature operating mode cases using the multiscale thermal-hydrologic model at the L5C3 location in the footprint of the potential repository. LTOM = lower-temperature operating mode.

Figure 5.3.1.4.11-3. Temperature and Relative Humidity Histories at the Waste Package Surface for Three Lower-Temperature Operating Mode Designs

C34

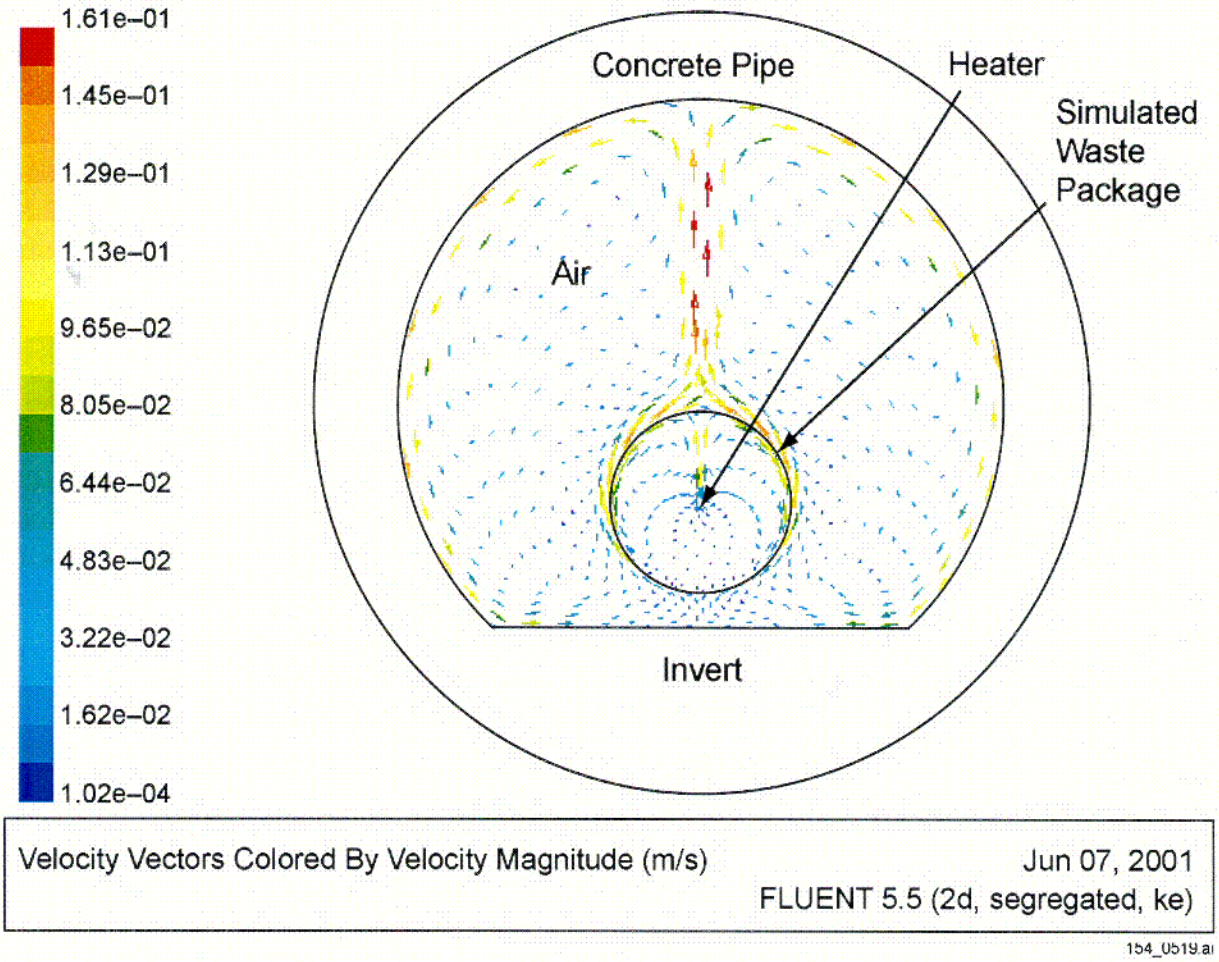

154_0519.ai

Source: Produced using files from Dunn 2001 [DIRS 155308].

NOTE: Similar patterns are expected to develop above and below the drip shield.

Figure 5.3.2-1. Air Flow Pattern in a Prediction of a Quarter-Scale Test of In-Drift Convection

C35

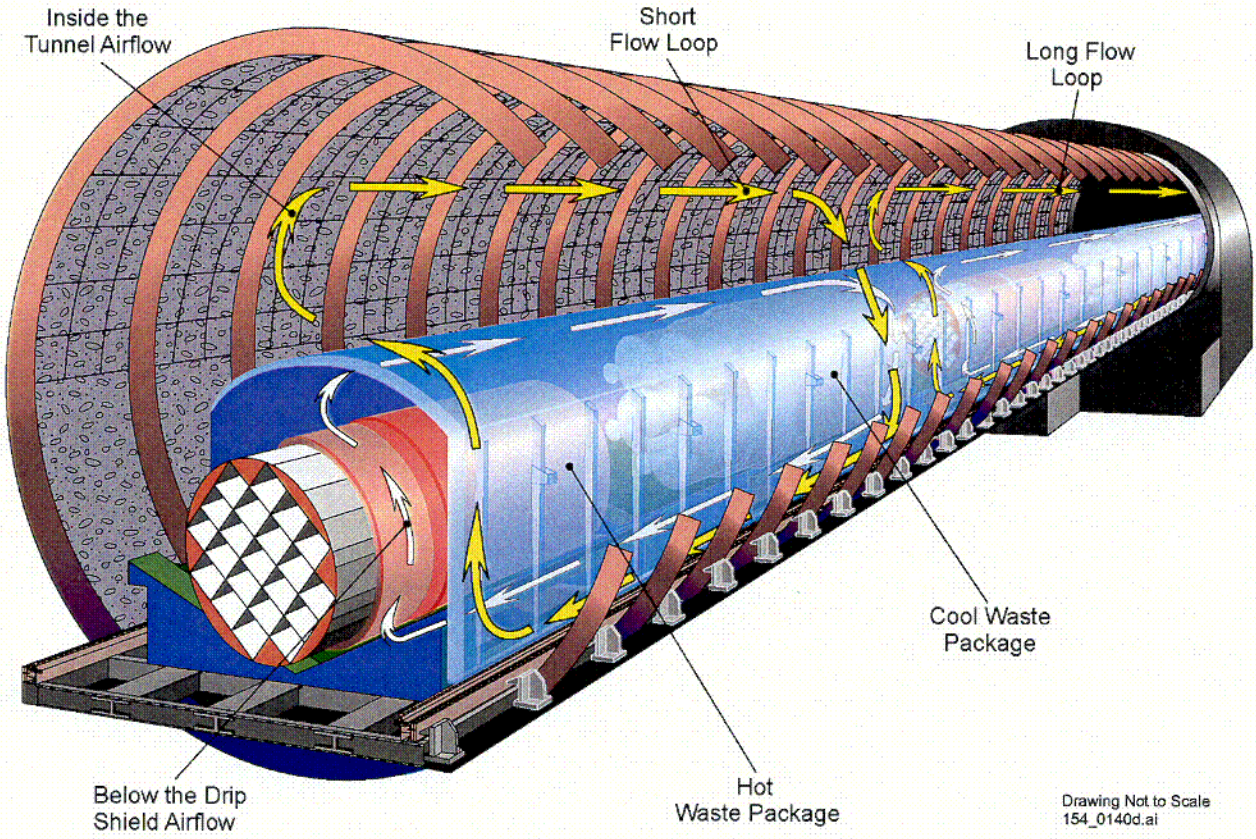

154_0140d.ai

Source: Adapted from CRWMS M&O 2001 [DIRS 154771], p.48.

Figure 5.3.2-2. Three-Dimensional Air Flow in a Closed Emplacement Drift

C36

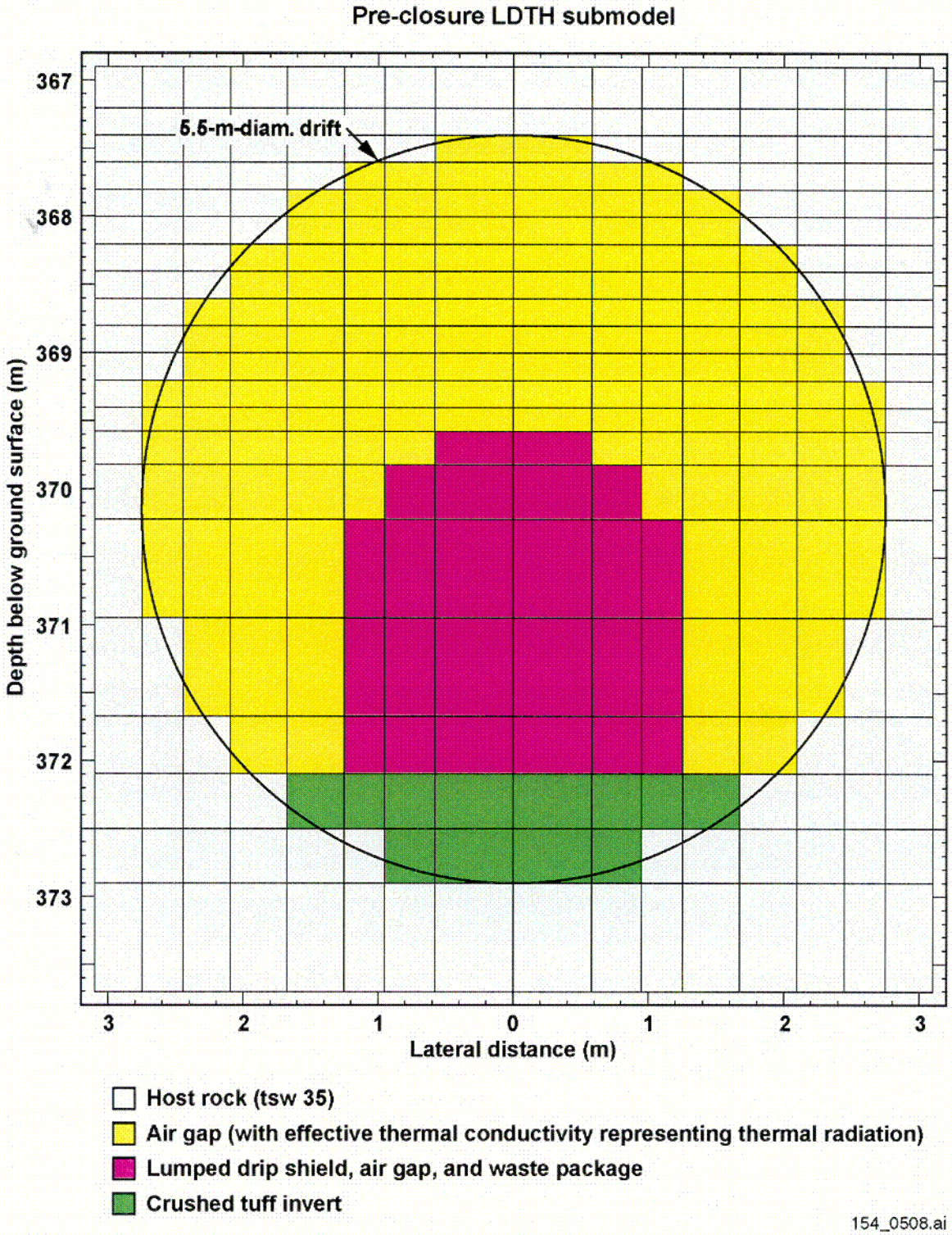

154_0508.ai

Source: Modified from CRWMS M&O 2000 [DIRS 149862], Figure 6-2, using updated invert dimensions and vertical location for one location in the repository.

NOTE: The values on the vertical axis shift with location within the potential repository footprint.

Figure 5.3.2.3-1. Numerical Mesh Used in the Line-Source Drift-Scale Thermal-Hydrologic Submodels

C37

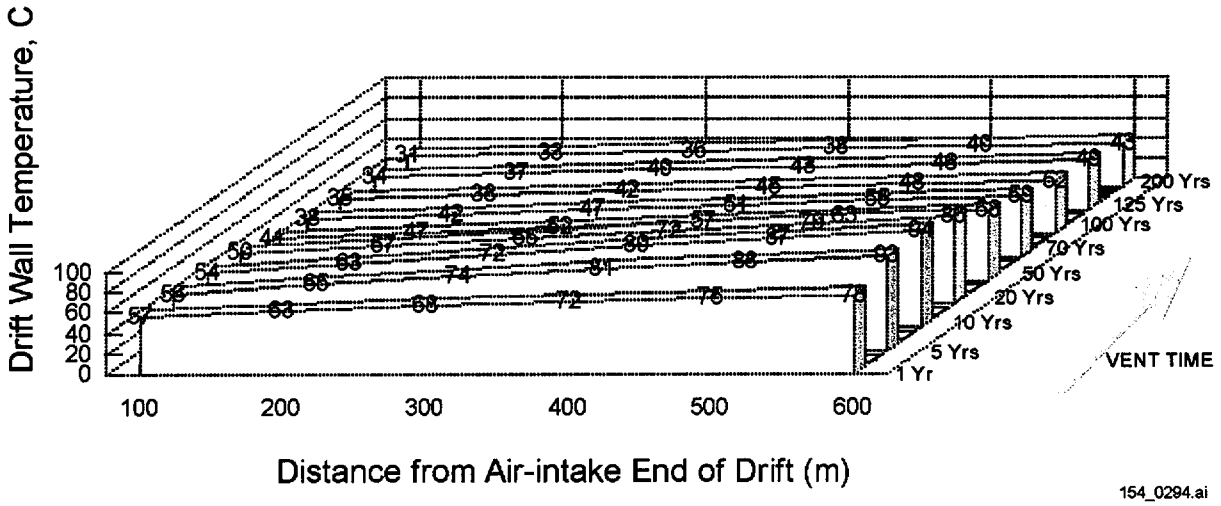

154_0294.ai

Source: CRWMS M&O 2000 [DIRS 120903], Figure 4.

Figure 5.3.2.4.1-1. Wall Temperature During Continuous Ventilation at 10 m^3/s

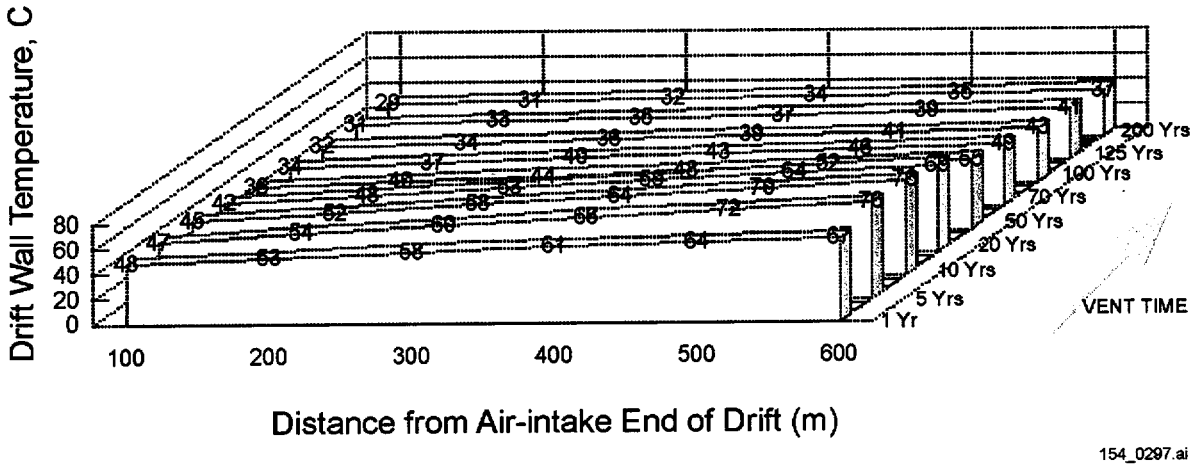

154_0297.ai

Source: CRWMS M&O 2000 [DIRS 120903], Figure 7.

Figure 5.3.2.4.1-2. Wall Temperature During Continuous Ventilation at 15 m^3/s

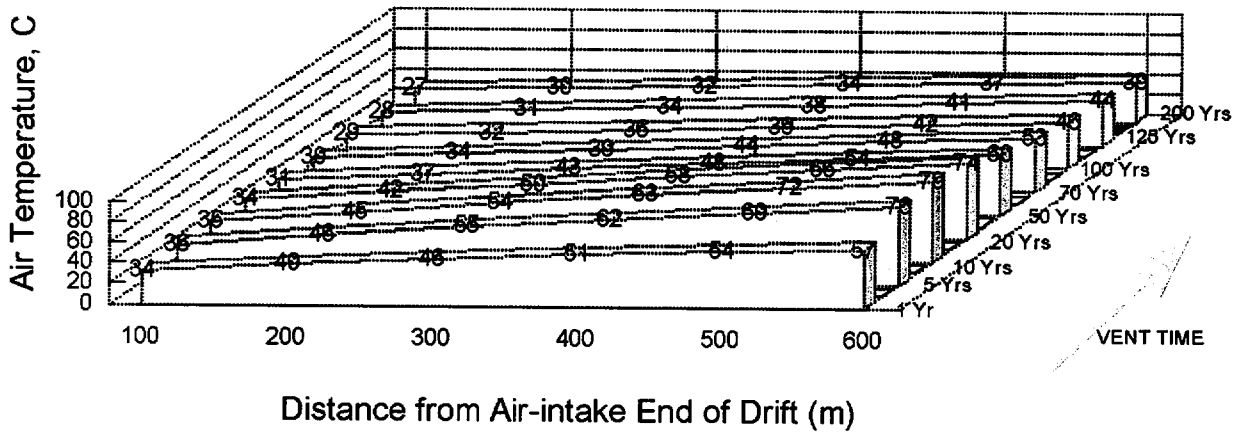

154_0295.ai

Source: CRWMS M&O 2000 [DIRS 120903], Figure 5.

Figure 5.3.2.4.1-3. Air Temperature During Continuous Ventilation at 10 m^3/s

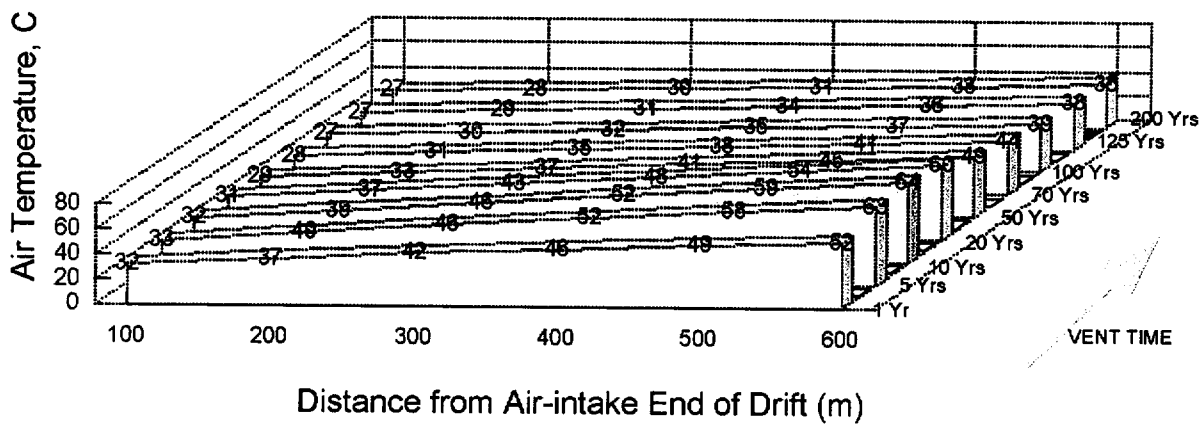

154_0298.ai

Source: CRWMS M&O 2000 [DIRS 120903], Figure 8.

Figure 5.3.2.4.1-4. Air Temperature During Continuous Ventilation at 15 m^3/s

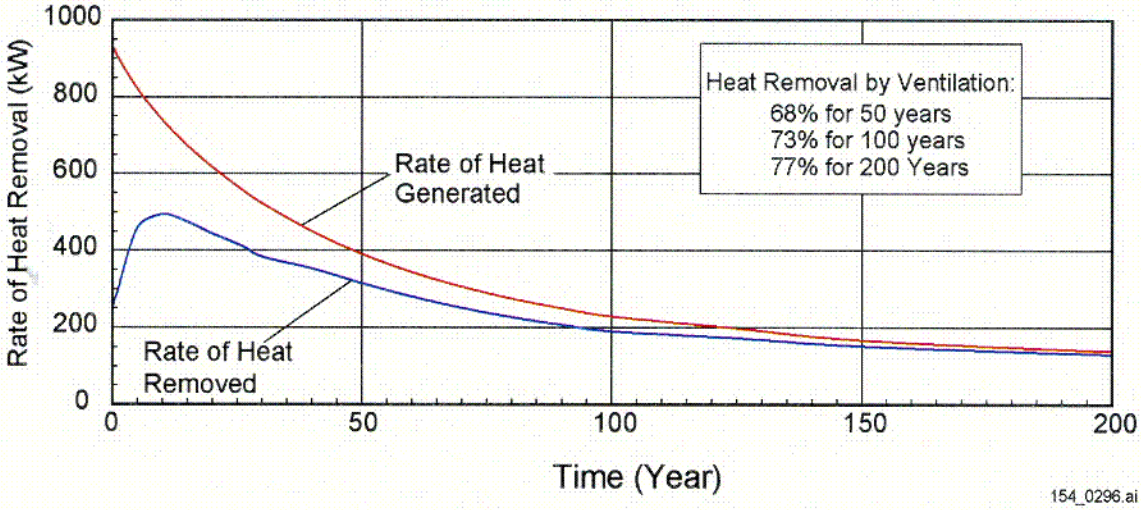

154_0296.ai

Source: CRWMS M&O 2000 [DIRS 120903], Figure 9.

Figure 5.3.2.4.1-5. Heat Removed During Continuous Ventilation at 10 m^3/s

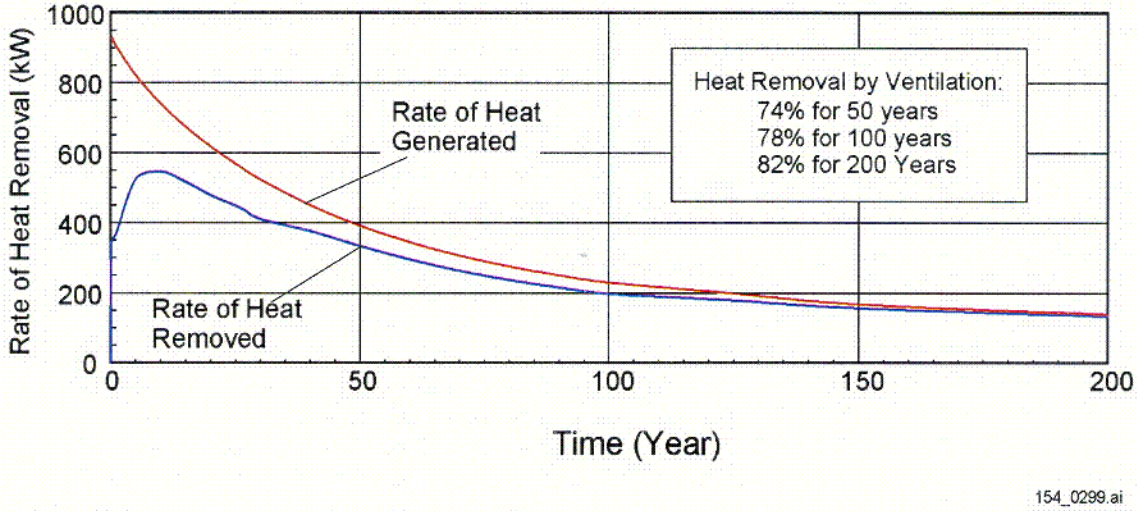

154_0299.ai

Source: CRWMS M&O 2000 [DIRS 120903], Figure 9.

Figure 5.3.2.4.1-6. Heat Removed During Continuous Ventilation at 15 m^3/s

C38

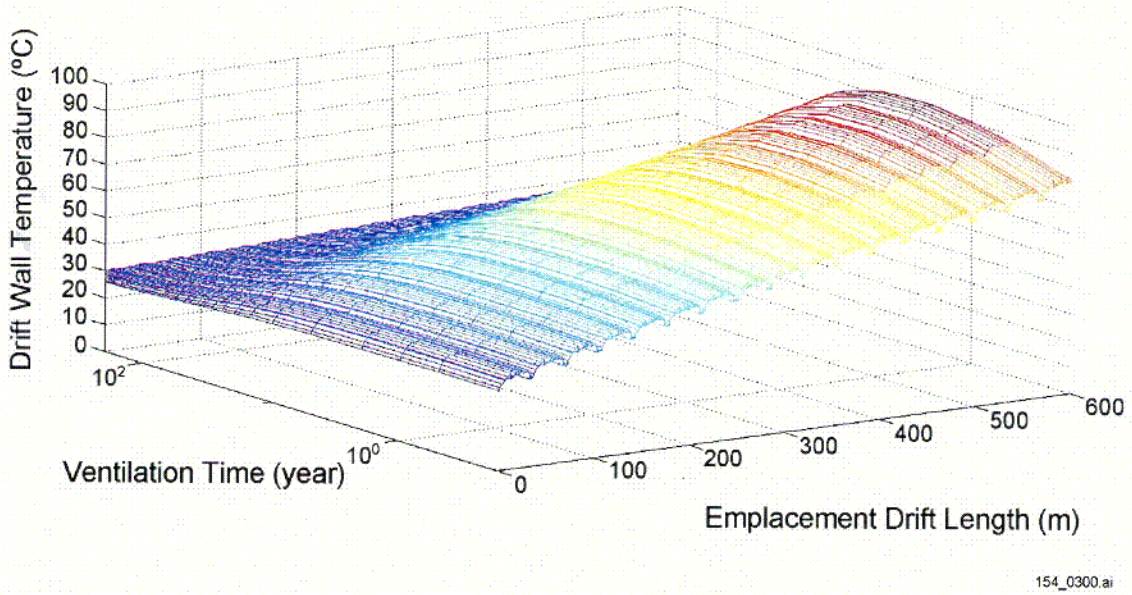

154_0300.ai

Source: BSC 2001 [DIRS 155025], Figure 10.

NOTE: MULTIFLUX Results.

Figure 5.3.2.4.1-7. Wall Temperature During Continuous Ventilation of 10 m^3/s

C39

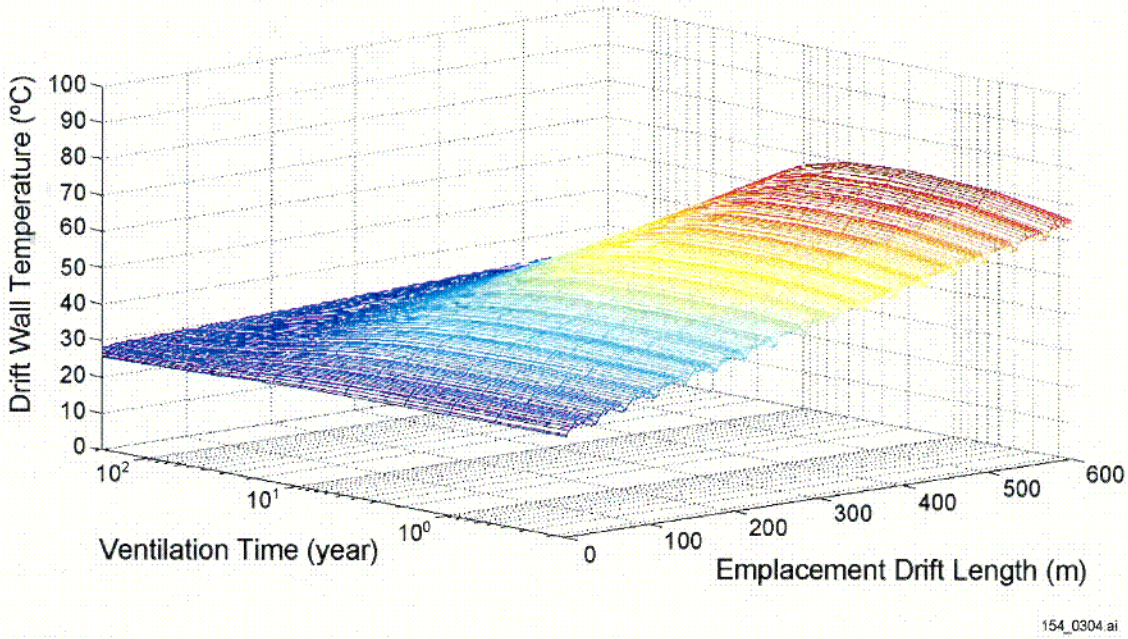

154_0304.ai

Source: BSC 2001 [DIRS 155025], Figure 14.

NOTE: MULTIFLUX Results.

Figure 5.3.2.4.1-8. Wall Temperature During Continuous Ventilation of 15 m^3/s

C40

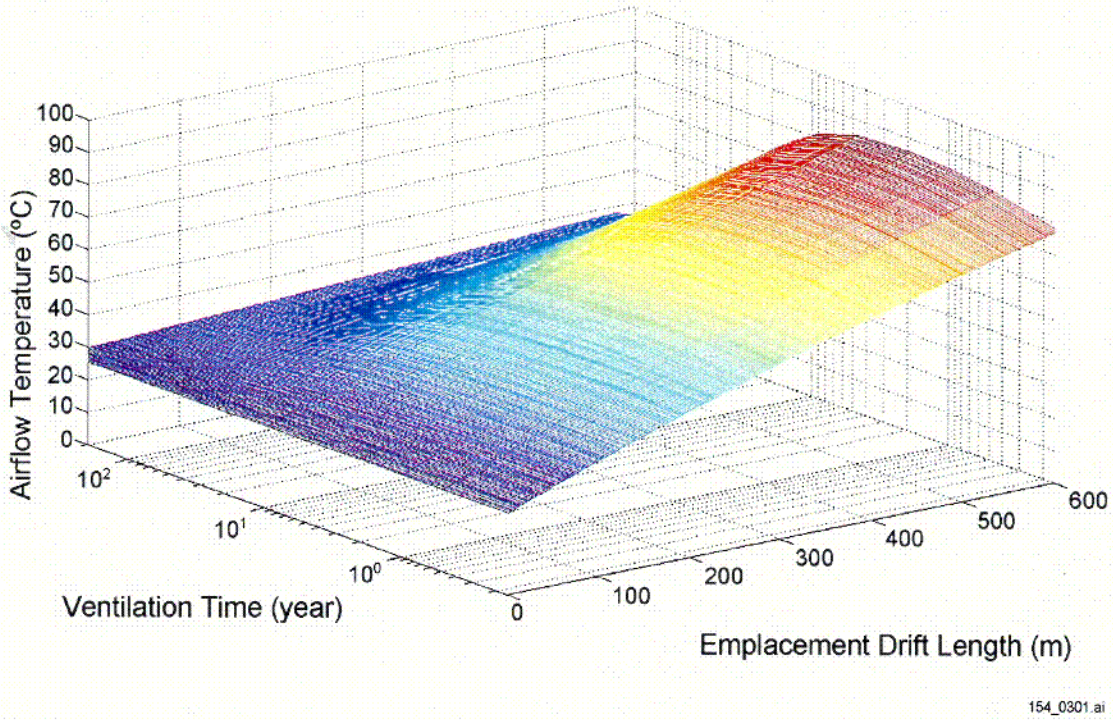

154_0301.ai

Source: BSC 2001 [DIRS 155025], Figure 11

NOTE: MULTIFLUX Results.

Figure 5.3.2.4.1-9. Airflow Temperature During Continuous Ventilation of 10 m^3/s

C41

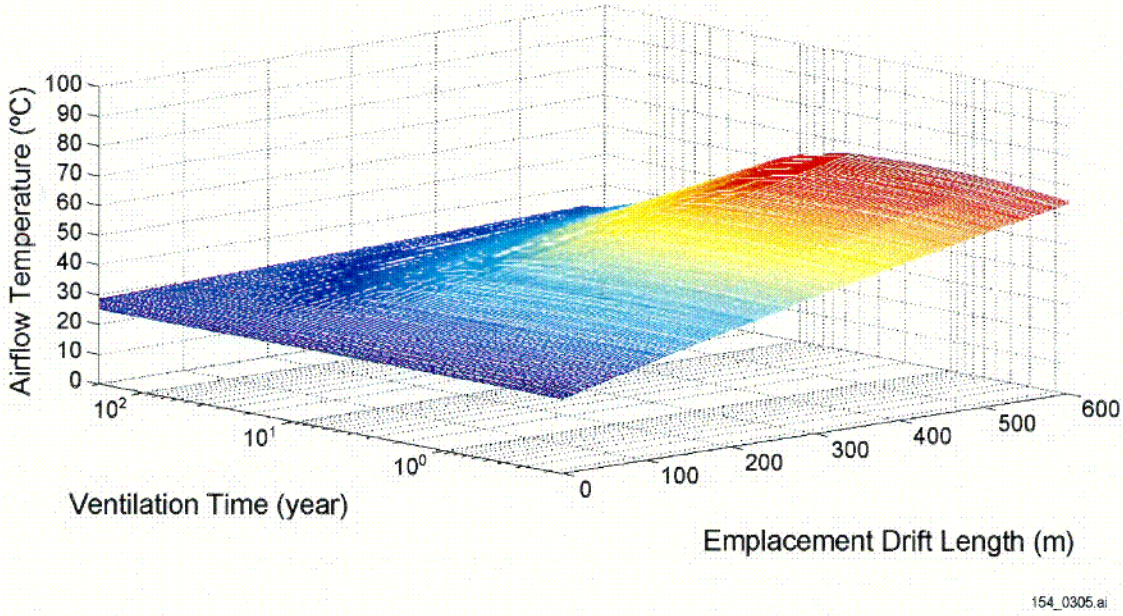

154_0305.ai

Source: BSC 2001 [DIRS 155025], Figure 15.

NOTE: MULTIFLUX Results.

Figure 5.3.2.4.1-10. Airflow Temperature During Continuous Ventilation of 15 m^3/s

C42

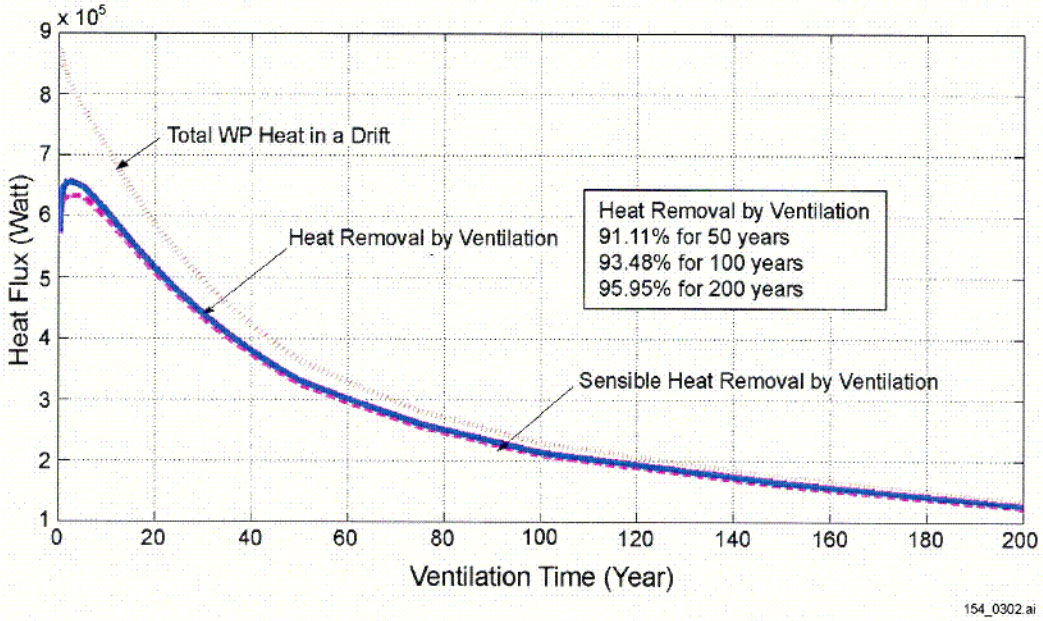

154_0302.ai

Source: BSC 2001 [DIRS 155025], Figure 12.

NOTE: MULTIFLUX Results.

Figure 5.3.2.4.1-11. Heat Removed During Continuous Ventilation of 10 m^3/s

C43

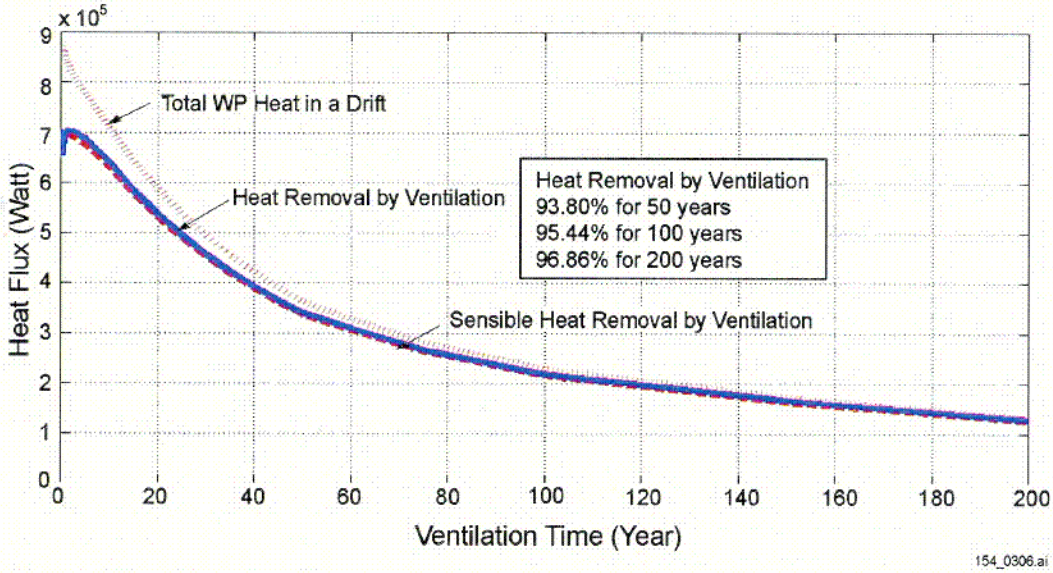

154_0306.ai

Source: BSC 2001 [DIRS 155025], Figure 16.

NOTE: MULTIFLUX Results.

Figure 5.3.2.4.1-12. Heat Removed During Continuous Ventilation of 15 m^3/s

C44

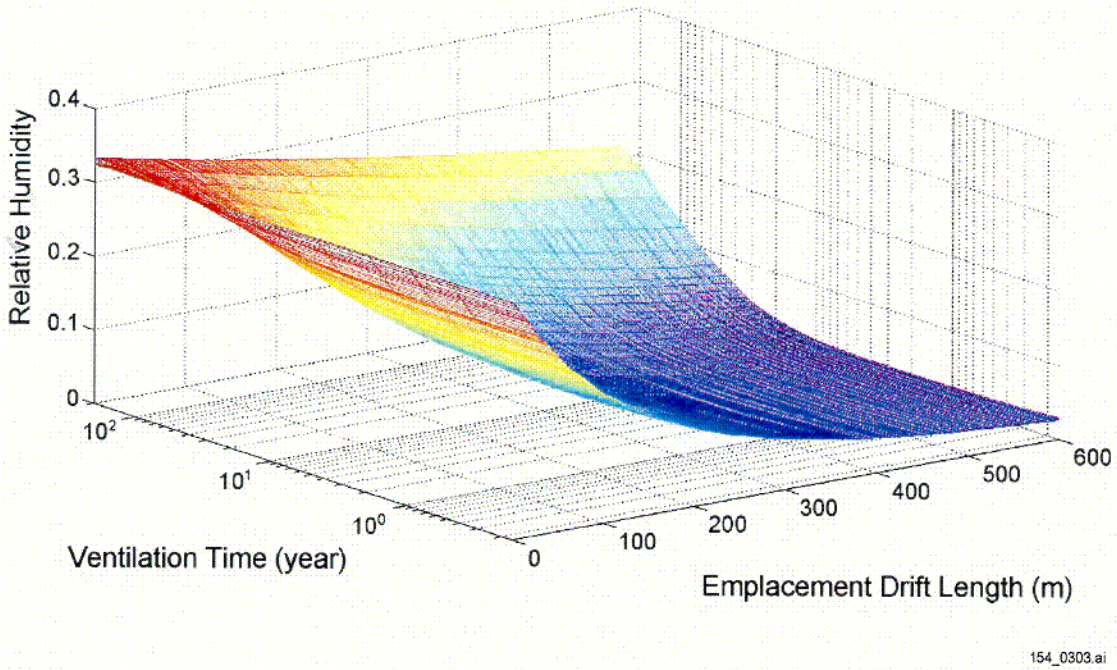

154_0303.ai

Source: BSC 2001 [DIRS 155025], Figure 13.

NOTE: MULTIFLUX Results.

Figure 5.3.2.4.1-13. Relative Humidity During Continuous Ventilation of 10 m^3/s

C45

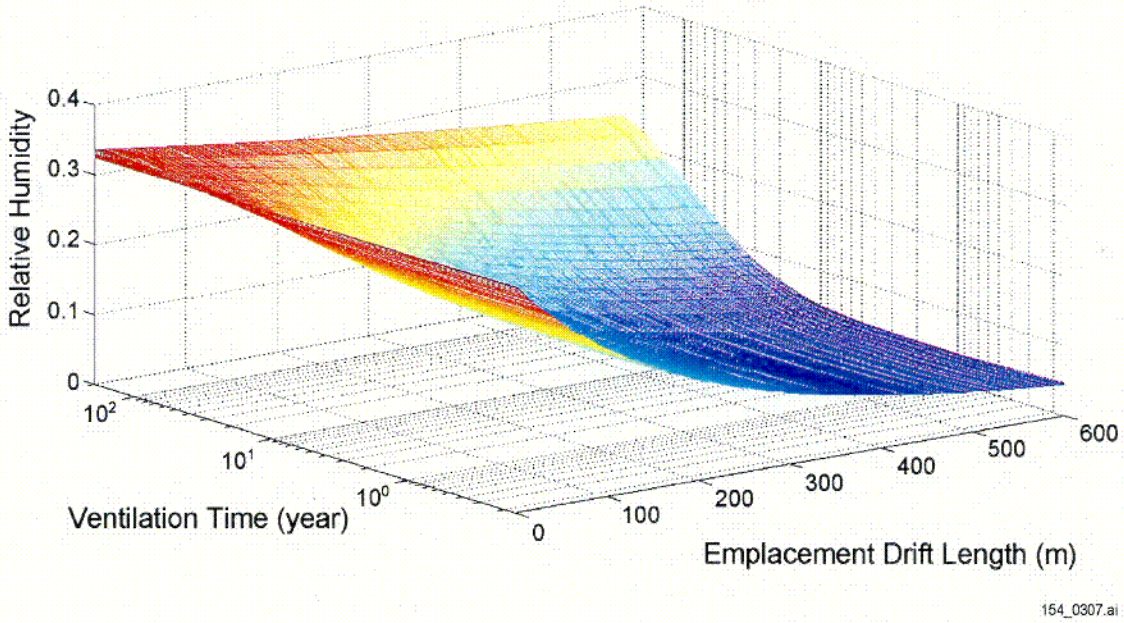

154_0307.ai

Source: BSC 2001 [DIRS 155025], Figure 17.

NOTE: MULTIFLUX Results.

Figure 5.3.2.4.1-14. Relative Humidity During Continuous Ventilation of 15 m^3/s

C46

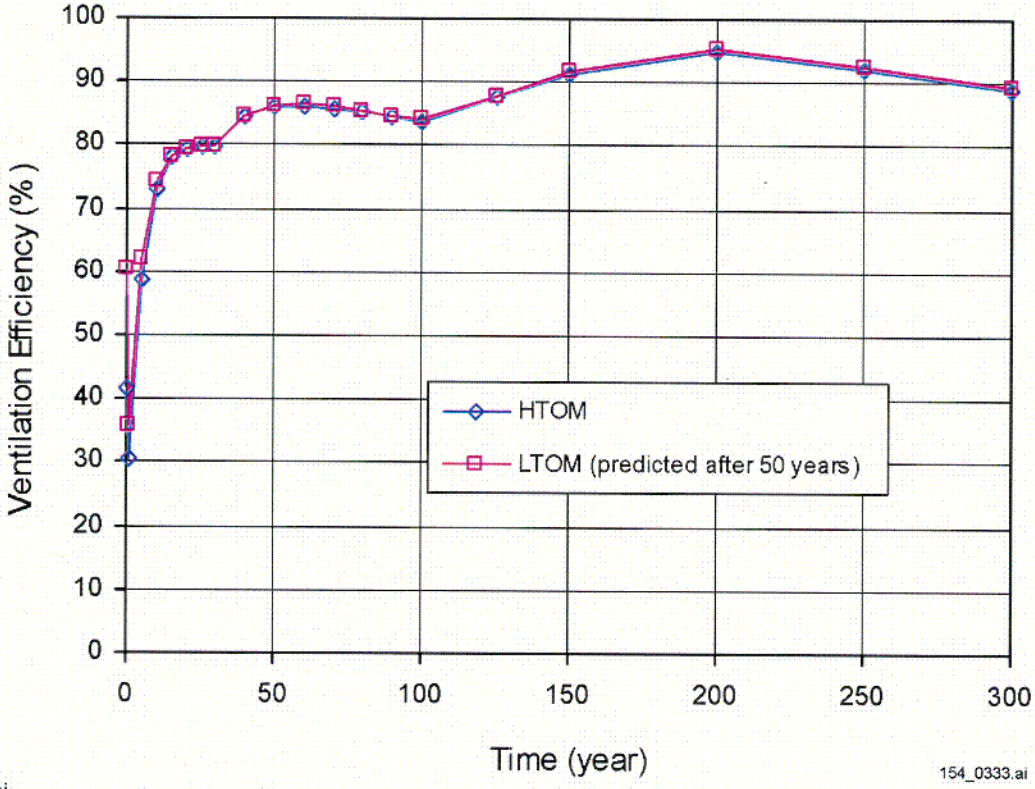

154_0333.ai

Source: Produced using files from Leem 2001 [DIRS 154996].

NOTE: HTOM = higher-temperature operating mode; LTOM = lower-temperature operating mode.

Figure 5.3.2.4.2-1. Time-Dependent Ventilation Efficiencies for the Higher- and Lower-Temperature Operating Modes

C47

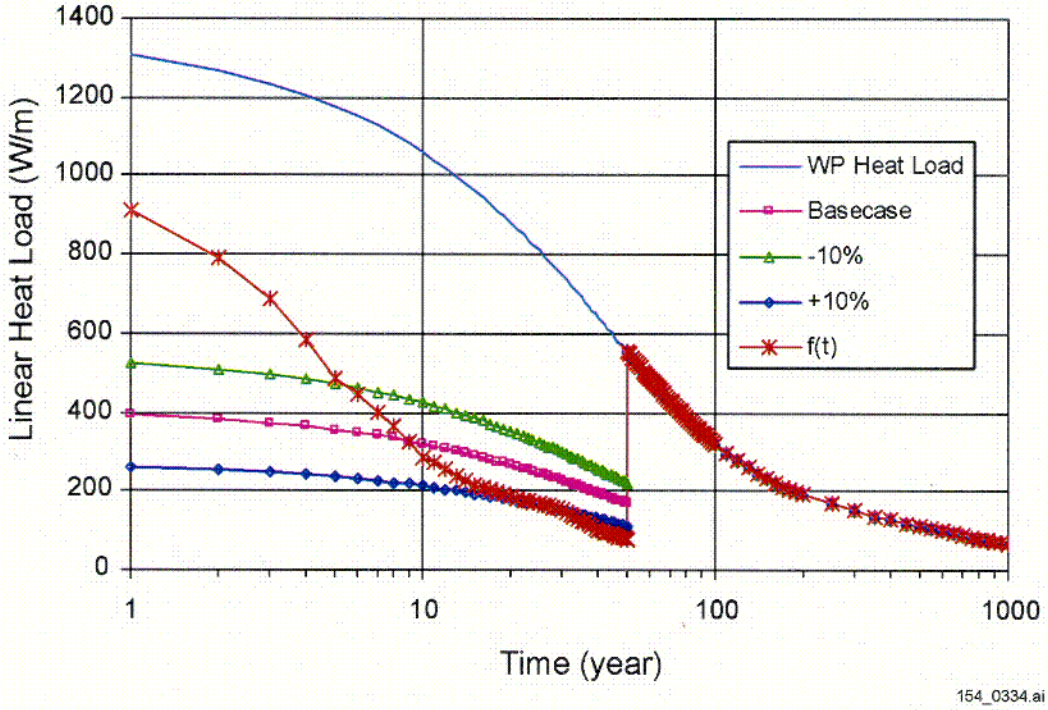

154_0334.ai

Source: Produced using files from Leem 2001 [DIRS 154996].

NOTE: WP = waste package.

Figure 5.3.2.4.2-2. Time History of Heat Available to Enter the Near-Field Rock for the Higher-Temperature Operating Mode Ventilation Cases

C48

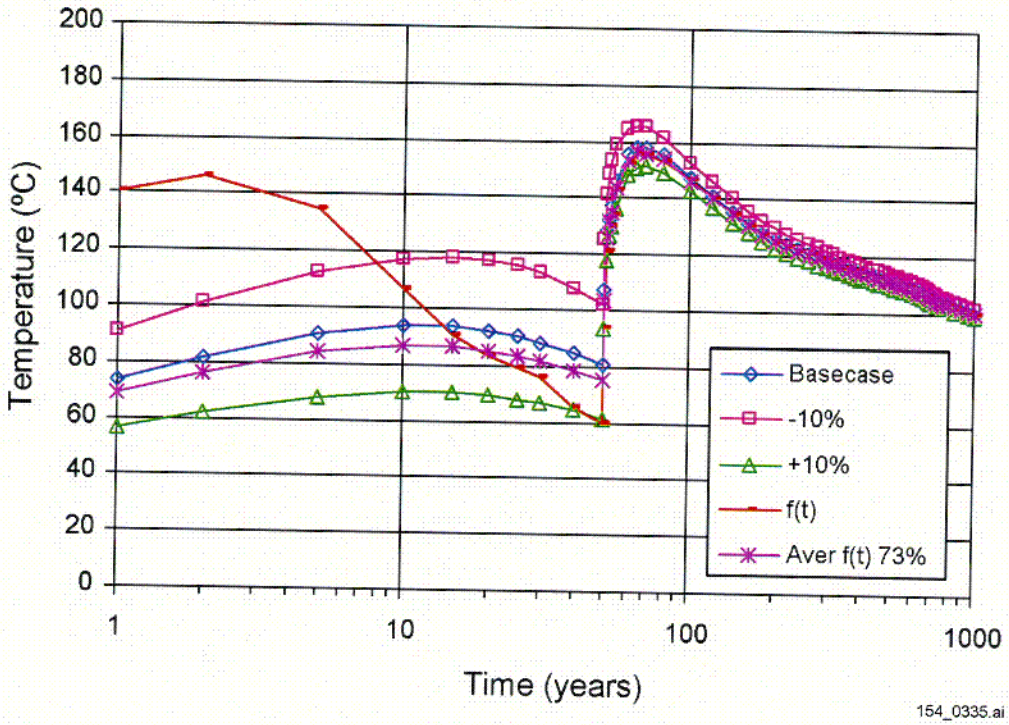

154_0335.ai

Source: Produced using files from Leem 2001 [DIRS 154996].

NOTE: Temperature histories presented as a function of ventilation efficiency.

Figure 5.3.2.4.2-3. Drip Shield Top Temperature Histories for the Higher-Temperature Operating Mode

C49

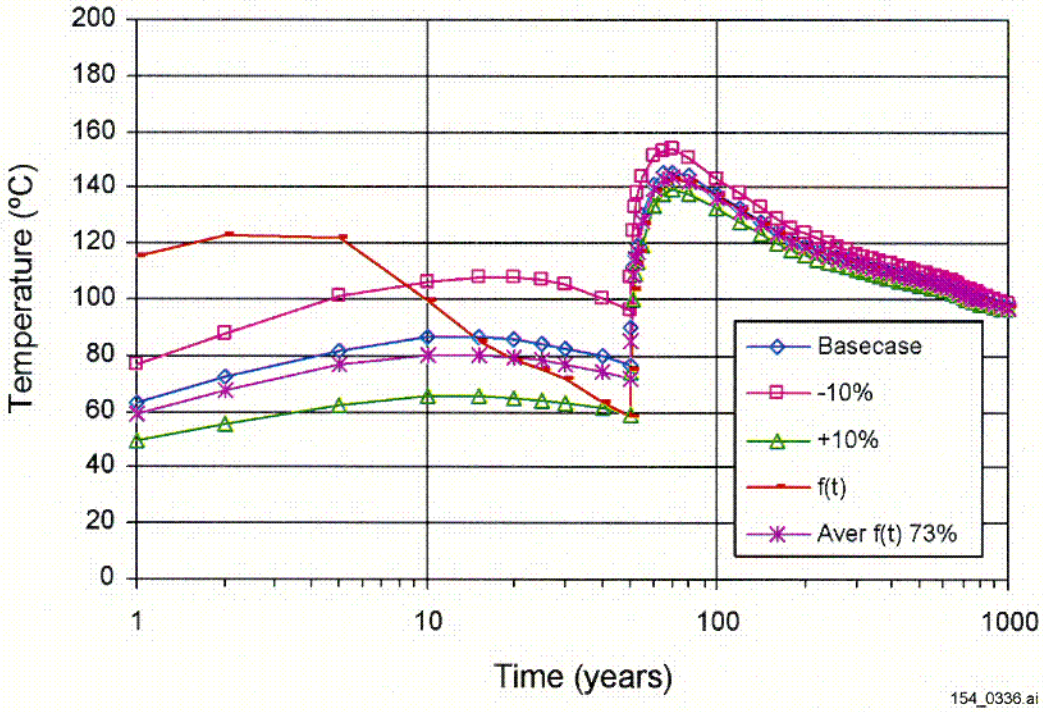

154_0336.ai

Source: Produced using files from Leem 2001 [DIRS 154996].

NOTE: Temperature histories presented as a function of ventilation efficiency.

Figure 5.3.2.4.2-4. Drift Wall Crown Temperature Histories for the Higher-Temperature Operating Mode

C50

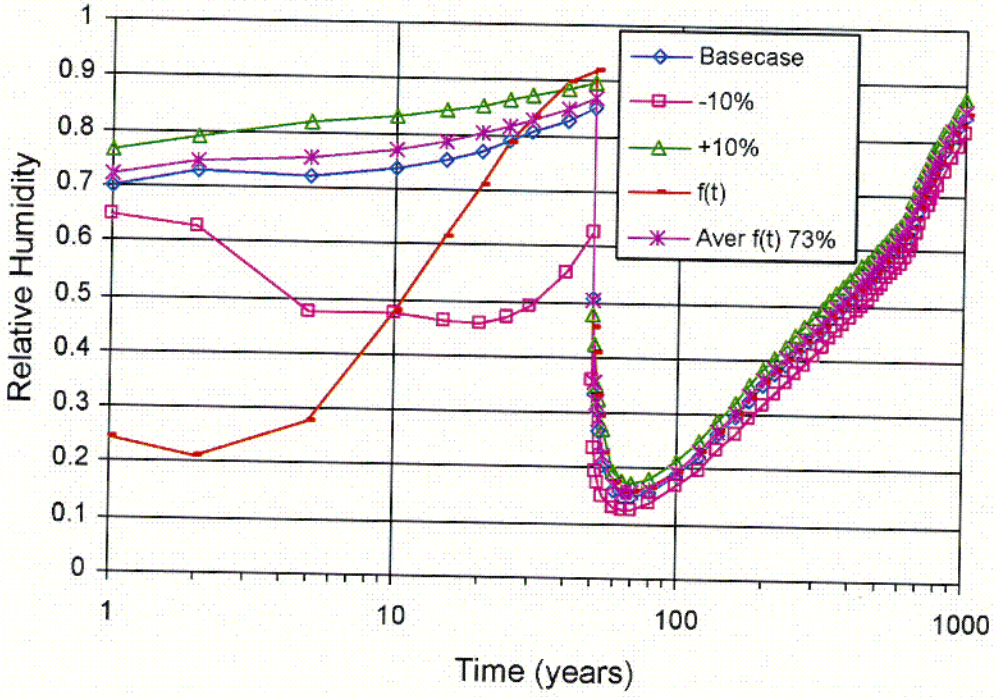

154_0337.ai

154_0337

Source: Produced using files from Leem 2001 [DIRS 154996].

NOTE: Relative humidity histories presented as a function of ventilation efficiency.

Figure 5.3.2.4.2-5. Drip Shield Top Relative Humidity Histories for the Higher-Temperature Operating Mode

C51